Dynamic changes in sulfate sulfur isotopes preceding the Ediacaran Shuram Excursion

Magdalena R. Osburn [a,c,*], Jeremy Owens [b,d], Kristin D. Bergmann [a,e], Timothy W. Lyons [b], John P. Grotzinger [a]

[a] *Division of Geological and Planetary Sciences, California Institute of Technology, Pasadena, CA 91125, USA*
[b] *Department of Earth Sciences, University of California, Riverside, CA 92521, USA*
[c] *Department of Earth and Planetary Sciences, Northwestern University, Evanston, IL 60208, USA*
[d] *Geology and Geophysics Department, Woods Hole Oceanographic Institution, Woods Hole, MA 025343, USA*
[e] *Department of Earth, Atmospheric and Planetary Sciences, Massachusetts Institute of Technology, Cambridge, MA 02139, USA*

Abstract

Large excursions in $\delta^{13}C$ and $\delta^{34}S$ are found in sedimentary rocks from the Ediacaran Period that may provide detailed mechanistic information about oxidation of Earth's surface. However, poor stratigraphic resolution and diagenetic concerns have thus far limited the interpretation of these records. Here, we present a high-resolution record of carbon and sulfur isotopes from the Khufai Formation, leading up to and including the onset of the Shuram carbon isotope excursion. We document large coherent excursions in the sulfur isotope composition and concentration of carbonate-associated sulfate (CAS) that occur both independently and synchronously with the carbon isotope excursion. Isotopic changes appear decoupled from major stratigraphic surfaces and facies changes, suggesting regional or global processes rather than local controls. Our data suggest that very low marine sulfate concentrations are maintained at least through the middle-Khufai Formation and require that the burial fraction of pyrite and the fractionation factor between sulfate and pyrite necessarily change through deposition. Reconciliation of simultaneous, up-section increases in marine sulfate concentration and $\delta^{34}S_{CAS}$ requires the introduction of strongly ^{34}S-enriched sulfate, possibly from weathering of Cryogenian and earlier Ediacaran ^{34}S-enriched pyrite. Our analysis of the onset of the Shuram carbon isotope excursion, observed in stratigraphic and lithologic context, is not consistent with diagenetic or authigenic formation mechanisms. Instead, we observe a contemporaneous negative excursion in sulfate $\delta^{34}S$ suggesting linked primary perturbations to the carbon and sulfur isotope systems. This work further constrains the size, isotopic composition, and potential input fluxes of the Ediacaran marine sulfate reservoir, placing mechanistic constraints on possible drivers of extreme isotopic perturbations during this critical period in Earth history.
© 2015 Elsevier Ltd. All rights reserved.

1. INTRODUCTION

The Neoproterozoic Era was a time of intense environmental and biological variability that included at least two significant glaciations (Wright et al., 1990; Hoffman et al., 1998; Macdonald et al., 2010; Halverson and Shields-Zhou, 2011), significant changes in deep ocean chemistry (Claypool et al., 1980; Strauss, 1993, 1997; Fike et al., 2006; Canfield et al., 2007, 2008; Lyons et al., 2012, 2014), and a number of evolutionary radiations and extinctions (Amthor et al., 2003; Narbonne, 2005; Love et al., 2009). The Ediacaran Period is particularly important in that it witnesses the demise of global glaciation, the onset

of early animal evolution, and likely at least episodic oxygenation of the deep ocean (Hurtgen et al., 2004; Xiao, 2004; Fike et al., 2006; Canfield et al., 2007; Scott et al., 2008; Shen et al., 2008b; Maloof et al., 2010; Erwin et al., 2011; Sahoo et al., 2012; Lenton et al., 2014). Evidence for these geochemical changes comes from perturbations to isotopic systems (C, S, etc.) and changes in inorganic geochemical proxies (REE, iron speciation) measured from sedimentary deposits (Kaufman et al., 1997; Hurtgen et al., 2002; Bartley and Kah, 2004; Halverson and Hurtgen, 2007; Schröder and Grotzinger, 2007; Fike and Grotzinger, 2008; Canfield et al., 2008; McFadden et al., 2008; Halverson et al., 2010; Johnston et al., 2012).

One such Ediacaran isotopic perturbation is the Shuram Excursion, the largest negative carbon isotope excursion in Earth history in terms of both magnitude and duration (Grotzinger et al., 2011, and references therein). This excursion is observed globally in multiple ocean basins, including Oman, South China, Death Valley/northern Mexico, Australia, and Namibia (Burns and Matter, 1993; Narbonne et al., 1994; Calver, 2000; Corsetti and Kaufman, 2003; Zhu et al., 2007; Melezhik et al., 2009; Le Guerroue et al., 2006a,b; Le Guerroue, 2010; Kaufman et al., 2007; McFadden et al., 2008; Prave et al., 2009; Verdel et al., 2011). The excursion is defined by a dramatic drop in $\delta^{13}C_{carb}$ from high values ($\sim6‰$) characteristic of the Ediacaran to as low as $-12‰$. A protracted recovery period, which could be as long as 50 Ma (million years), covers a range of sedimentary environments (Le Guerroue et al., 2006b). While a number of diagenetic mechanisms have been suggested (Knauth and Kennedy, 2009; Derry, 2010; Schrag et al., 2013), none can account for the global occurrence of strikingly similar excursions across diverse sedimentary environments (Grotzinger et al., 2011). Primary (non-diagenetic) mechanisms to explain the Shuram Excursion are varied and controversial but broadly center on a large scale oxidation event (Rothman et al., 2003; Fike et al., 2006; Kaufman et al., 2007; McFadden et al., 2008; Grotzinger et al., 2011) and recently a bolide hypothesis (Young, 2013). Globally, the Shuram Excursion is found in a transgressive package (Le Guerroue et al., 2006a,b; Bergmann et al., 2011), or highly condensed section (McFadden et al., 2008), which limits stratigraphic resolution; in some cases the initial $\delta^{13}C$ decline is missed entirely (Loyd et al., 2012a,b). The Khufai Formation, the focus of this study, provides a record up to and including the excursion onset, alleviating some of these concerns.

The carbon and sulfur cycles are mechanistically linked, often co-recording perturbations to the Earth system, although with different timescales and sensitivities (e.g., Garrels and Lerman, 1981). It is perhaps reasonable then that the Ediacaran sulfur isotope record is volatile, recording large excursions in both sulfate and sulfides (Fike et al., 2006; Halverson and Hurtgen, 2007; Fike and Grotzinger, 2008). Fike et al. (2006) present carbon and sulfur isotope data from the duration of the Shuram Excursion and observe relative consistency in $\delta^{34}S_{CAS}$ at $\sim25‰$ during the excursion but very large variations beforehand, including at the excursion onset (Fike et al., 2006). However, the limited resolution of these data and lack of paired

sedimentological observations precluded further interpretation of this tantalizing dataset. Loyd et al. (2012a,b) observe a pronounced decline in $\delta^{34}S_{CAS}$ and increase in CAS concentration ([CAS]) coincident with the $\delta^{13}C$ decline in Mexico, but their interpretations were challenged by the lack carbonate facies lower in the unit. The veracity of $\delta^{34}S_{CAS}$ excursions and timing of the increase in [CAS] relative to the global isotopic signal remain open questions.

The Khufai Formation, Sultanate of Oman, records the onset of the Shuram Excursion as well as the pre-excursion conditions in a ~300 m-thick package of carbonate rocks, representing semi-continuous deposition (Osburn et al., 2014). This section is the most expanded and continuous known record of carbonate sedimentation recording the initial isotopic decline and, as such, represents an ideal target for detailed observation of the environmental conditions prior to and during the initial excursion. Here, we present a high-resolution paired carbon and sulfur isotope record of the Khufai Formation demonstrating large excursions in sulfur isotope ratios both preceding and coincident with the well-documented carbon isotope excursion.

2. BACKGROUND: S-ISOTOPE AND CONCENTRATION PROXIES

The record of sulfur isotopes through time is derived from measurements of marine evaporites and trace sulfate incorporated into the matrix of carbonate minerals (carbonate-associated sulfate; CAS) (Claypool et al., 1980; Burdett et al., 1989; Strauss, 1993, 1997; Kampschulte and Strauss, 2004) and barite analysis in younger samples (Paytan et al., 1998, 2004). Development of the CAS method has expanded the available record of Precambrian sulfur isotope data considerably and in many cases reveals large magnitude isotopic excursions and examples of rapid isotopic variability (Hurtgen et al., 2004; Kah et al., 2004; Gellatly and Lyons, 2005). While subject to diagenetic processes, this technique has been shown to faithfully record isotopic compositions from the modern ocean (Kampschulte and Strauss, 2004) and broadly agrees with evaporite records where both are available (Strauss, 1997; Kah et al., 2004). In addition, recrystallization from aragonite to calcite can preserve sulfur isotope ratios while decreasing residual CAS concentration (Gill et al., 2008). Evaporite and CAS records consistently suggest that the latest Precambrian was a time of highly variable but generally increasing $\delta^{34}S_{CAS}$ preceding the extreme excursions observed near the Precambrian–Cambrian boundary (Fike et al., 2006; Fike and Grotzinger, 2008, 2010; Halverson et al., 2010). These rapid and high magnitude changes in $\delta^{34}S_{CAS}$ have been interpreted to suggest low marine sulfate concentrations, while the increasing $\delta^{34}S_{CAS}$ values may indicate increased ocean oxidation (Fike et al., 2006; Fike and Grotzinger, 2008; Halverson et al., 2010).

Interpreting marine sulfate concentration through time is considerably more complex. Very generally, the limited occurrence of sulfate evaporites and low [CAS] in Precambrian strata suggest significantly lower sulfate concentrations than modern seawater (Strauss, 1997; Kah et al., 2004). Additional constraints are derived from the rate of

sulfur isotope change over particular stratigraphic intervals (e.g., Kah et al., 2004). Both CAS concentrations and $d\delta^{34}S/dt$-derived estimates in Precambrian rocks, including post-Marinoan strata, suggest a predominance of very low (<1 mM) sulfate concentrations (Hoffman et al., 1998; Hurtgen et al., 2002; Amthor et al., 2003; Narbonne, 2005; Kaufman et al., 2007; Macdonald et al., 2010; Loyd et al., 2012a,b; Wu et al., 2015). However, estimates based on evaporite deposits in Oman that span the Precambrian-Cambrian boundary suggest roughly modern values (16–25 mM) (Brennan et al., 2004; Fike and Grotzinger, 2008). These upper bounds require dramatic increases in marine sulfate concentration, at least locally, prior to the Cambrian boundary, as has been suggested previously (Halverson and Hurtgen, 2007; Wu et al., 2015) and is supported in greater detail and complexity by this study.

3. GEOLOGICAL SETTING

The Huqf Supergroup spans latest Cryogenian through earliest Cambrian time, cropping out in the Oman Mountains and the Huqf and Mirbat areas (Wright et al., 1990; Allen, 2007), and is accessed in the subsurface via hydrocarbon exploration wells (Forbes et al., 2010). In ascending order, the Huqf Supergroup is composed of the Hadash, Masirah Bay, Khufai, Shuram, and Buah formations capped with the Ara Group (Wright et al., 1990). The lower formations of the Huqf Supergroup consist of two siliciclastic-to-carbonate grand cycles, with the Khufai Formation defining the carbonate phase of the first cycle bounded above and below by marine siltstone and shales.

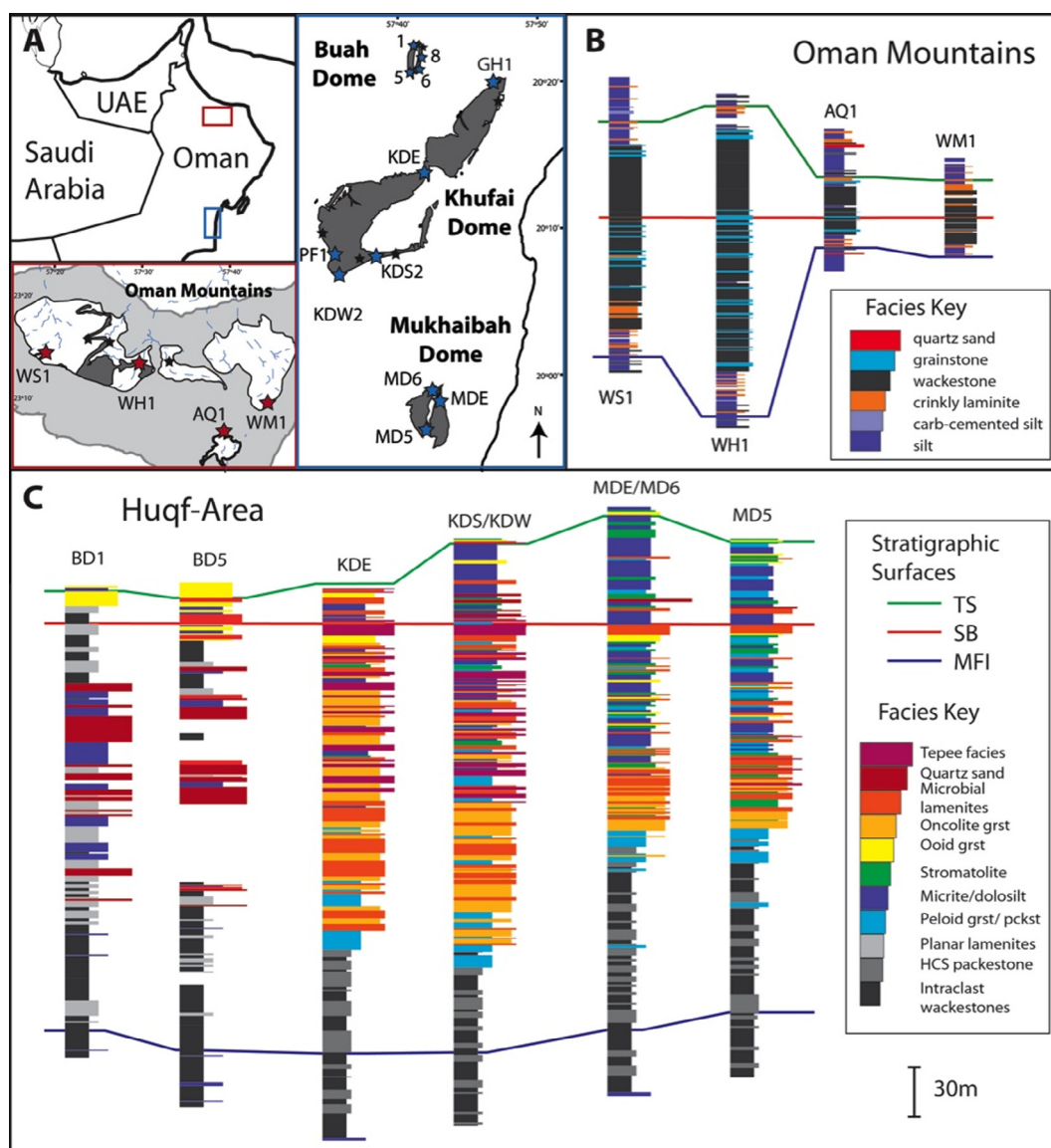The Khufai Formation was sampled in the Oman Mountains and the Huqf area of the central coast

Fig. 1. Geographic and stratigraphic information for the Khufai Formation. (A) Map showing the locations of the Oman Mountains and Huqf with expanded panels illustrating study sites (stars). (B) Stratigraphic summary of Oman Mountain sections with major sequence stratigraphic surfaces. (C) Stratigraphic summary of sections from the Huqf with stratigraphic surfaces.

(Fig. 1). Stratigraphic sections from the Oman Mountains preserve deep-water facies, including turbiditic wackestones and packstones, deep-water microbialites, and siliciclastic siltstone (Fig. 1b). In contrast, the stratigraphy of the Huqf area records a prograding carbonate platform with environments ranging from outer-ramp to supratidal (Osburn et al., 2014 and references therein). Depositional facies include a diversity of grainstone types, microbialites, and lagoonal deposits (Fig. 1c). Stratigraphic sections in the Huqf area are thick, ranging from 310 to 340 m compared to 50 to 185 m in the mountains. The sediments from the Huqf area are also better preserved than those of the Oman Mountains owing to shallower burial and minimal tectonic deformation (Osburn et al., 2014). A full stratigraphic characterization of the Khufai Formation is presented in Osburn et al. (2014).

4. MATERIALS AND METHODS

4.1. Sample collection and correlation

Samples were collected in 2009, 2010, 2011, and 2012 in concert with stratigraphic and sedimentologic field analysis. Samples for sulfur and carbonate isotope analysis were taken at $\sim$2 and 1 m intervals, respectively. Additional material was collected for slab and petrographic analysis of facies, described previously (Osburn et al., 2014). Section names, locations, stratigraphic thicknesses, and the isotopic analyses preformed are listed in Table A1.

In order to compare chemostratigraphic data, a normalized vertical scale (Z_n^*) was created from sequence stratigraphic boundaries defined for the Huqf and Oman Mountain areas. For the Huqf sections, the base and top of carbonate deposition were set to 0 and 320 m, respectively, and sixteen intermediate stratigraphic surfaces were used as tie points between sections. Z_n^* values for each section were calculated relative to the type section (MD5). These surfaces are sequence stratigraphic boundaries, and thus timelines, allowing for observation of contemporaneous chemical events. This exercise was repeated for Oman mountain sections using 0 and 120 m as upper and lower boundaries and six intervening calibration surfaces. For details on this approach see Osburn et al. (2014).

4.2. CAS extraction

Samples for sulfate extraction were first cleaned and trimmed to remove outer surfaces and visible secondary carbonate phases, such as cement filled veins, before crushing and powdering. All equipment was rinsed with MilliQ water and acetone before use and between samples. Approximately 60 g splits of powdered samples were weighed into 1 L Erlenmeyer flasks capped with glass watch glasses for CAS purification and extraction. CAS extraction followed a protocol modified from Burdett et al. (1989) and similar to Gill et al. (2011). Samples were rinsed as follows: 10% NaCl, MilliQ, 3% bleach, and MilliQ (2×), each occurring at least overnight, followed by removal of the overlying solution by decanting. After the final MilliQ rinse, samples were dissolved in 4 M HCl and filtered immediately on

0.4 μm nitrocellulose membrane filters (Millipore) to remove the insoluble fraction. The filtrate was adjusted to a known volume, and a 5 ml aliquot was removed for elemental analysis. The remaining sample was returned to a clean flask, and saturated $BaCl_2$ solution was added to precipitate dissolved sulfate as barite. The barites were filtered again onto 0.4 μm nitrocellulose membranes, dried, scraped, and stored until isotopic analysis.

4.3. Isotopic analyses

Carbon and oxygen isotope analyses were performed using standard isotope ratio mass spectrometry techniques coupled to either a ThermoScientific Keil IV or Gas Bench II sample preparation device. Hand samples were prepared by cutting to expose fresh surfaces and micro-drilled to produce $\sim$0.5 mg of powder. Areas with evidence for recrystallization and clear secondary phases were avoided. Carbon and oxygen isotope analyses were performed at five labs over four years: Washington University in St. Louis; University of Missouri; University of Michigan Stable Isotope Laboratory; University of California, Riverside; and the California Institute of Technology. Replicate samples were compared among the labs to maintain internal consistency. The standard deviation of replicate analyses of samples and standards averaged 0.036‰ for carbon and 0.045‰ for oxygen isotopes, although accuracy and precision on standards is generally reported at 0.1‰. All analyses are reported relative to Vienna Pee Dee Belemnite (VPDB).

Sulfur isotope analyses were performed at the University of California, Riverside, by EA-IRMS. Barite precipitates were homogenized and weighed into tin capsules with an excess of V_2O_5 for combustion via elemental analyzer. The resultant SO_2 was analyzed online for $^{34}S/^{32}S$ using a Thermo Delta V gas sourced IRMS. Sulfur isotope composition is reported in permil relative to Vienna Canyon Diablo Troilite (V-CDT) using the standard delta notation. Instrumental error on standards (NBS 127, IAEA SO-5, IAEA SO-6) and replicate samples was 0.2‰.

4.4. CAS concentration

The concentration of CAS in each sample was measured from aliquots of known volume taken immediately post dissolution. Samples were analyzed at the Biogeochemistry Laboratory at the University of California, Riverside, using an Agilent 7500ce quadrupole ICP-MS with Xe as the collision cell gas. Sulfate was measured as total S with error on replicates better than 5%. CAS concentration was corrected for the insoluble content of each sample.

5. RESULTS: FORMATION-SCALE CHEMOSTRATIGRAPHY

5.1. Data from the Huqf sections

Isotopic data from the Huqf region show remarkable continuity among the locations in both trend and magnitude (Fig. 2). $\delta^{13}C$ values among the sections for a given

stratigraphic height often agree to within ±1‰ of the running average, although samples from Buah Dome tend to diverge from the others. In ascending stratigraphic order, $\delta^{13}C$ values first increase slightly from ∼2 to >5‰. High values are maintained with a very slight negative slope for 250 m before decreasing rapidly to $\delta^{13}C$ values approaching −10‰ at the formation boundary. This decline defines the falling limb of the Shuram Isotope Excursion and does not recover to positive values until well into the Buah Formation (Burns and Matter, 1993; Le Guerroue et al., 2006b).

Oxygen isotope data show considerably more scatter through the sections; however, there is still a distinct pattern of consistency in stratigraphic trends among the sections. Despite the scatter, the majority of $\delta^{18}O$ values are high (−3‰ to −4‰). Samples from Buah Dome are significantly depleted relative to the other Oman sections, most significantly during the interval of highest $\delta^{18}O$ values elsewhere from 75 to 275 m.

Sulfur isotope composition and [CAS] show systematic trends in the Khufai Formation. $\delta^{34}S_{CAS}$ values begin at an average of 25‰ and decrease slightly over 75 m to 22‰. CAS concentration is broadly constant to slightly declining over this interval. Directly following this decline is a relatively rapid increase in $\delta^{34}S_{CAS}$ and [CAS] to 30‰ and ∼500 ppm, respectively, followed by a gradual decline

ending at Z_n^* 150 m. The most dramatic signals in both $\delta^{34}S_{CAS}$ and [CAS] occur between 150 and 310 m, where a strongly linear increase in $\delta^{34}S_{CAS}$ peaks at 35‰ and coincides with a dramatic, although highly variable, increase then decline in CAS concentration. Following this rise, the isotopic composition declines dramatically, synchronous with the onset of the Shuram carbon isotope excursion.

We will refer to the first increase–decrease in $\delta^{34}S_{CAS}$ as Khufai 1, the subsequent increase as Khufai 2, and the terminal decline as the Shuram Excursion for the remainder of this paper. The formation-scale sequence boundary identified in Osburn et al. (2014) is plotted behind the data in red lines for reference (Fig. 2). Notably, isotopic trends are invariant with respect to this boundary, with the sharp decline of the Shuram excursion beginning well after evidence for extensive exposure.

5.2. Data from the Oman Mountains

Carbon isotope trends from the Oman Mountains are broadly similar to those of the Huqf area (Fig. 3). They begin by increasing slightly up section to stable and high $\delta^{13}C$ values before decreasing near the sequence boundary. The heaviest $\delta^{13}C$ values are higher than in the Huqf (up to
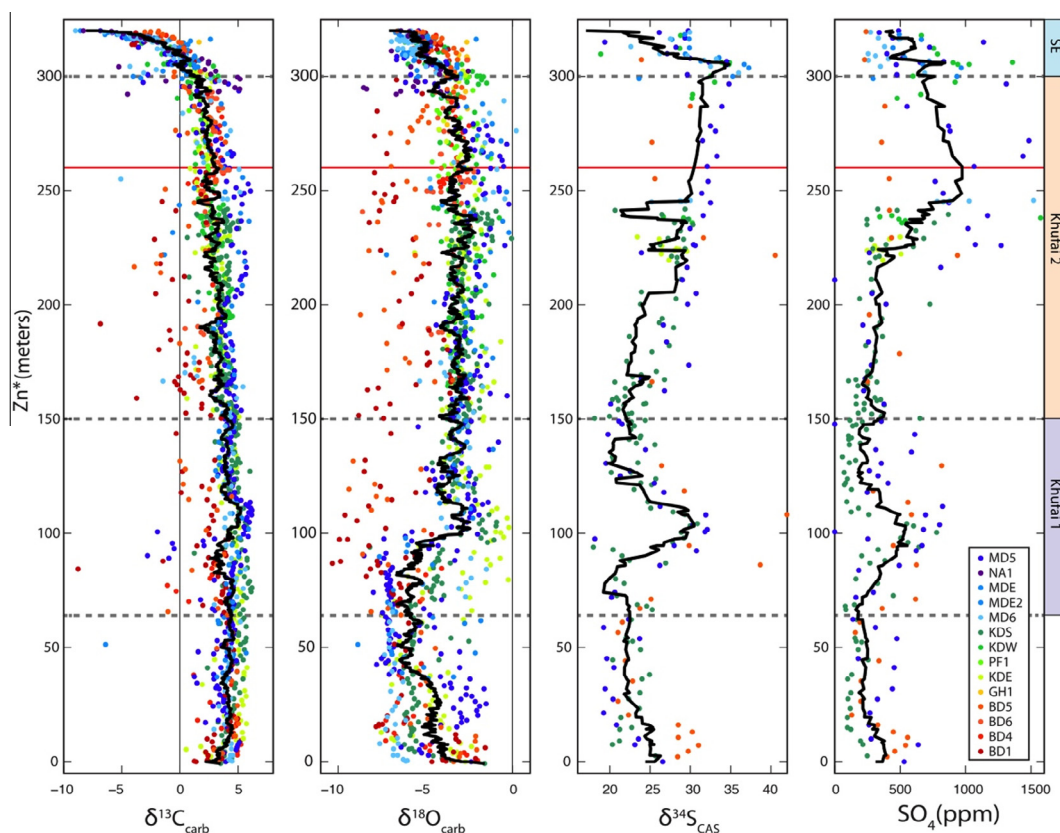

Fig. 2. Chemostratigraphic data for Huqf samples plotted against Zn^* (see text for details). Running averages ($N = 15$ for $\delta^{13}C$ and $\delta^{18}O$, $N = 10$ for $\delta^{34}S$ and SO_4) of data from all areas are shown in solid black lines. Khufai 1, 2, and the onset of the Shuram Excursion (SE) are indicated to the right and by dashed gray lines. The accommodation minimum is shown in the red line. (For interpretation of the references to color in this figure legend, the reader is referred to the web version of this article.)
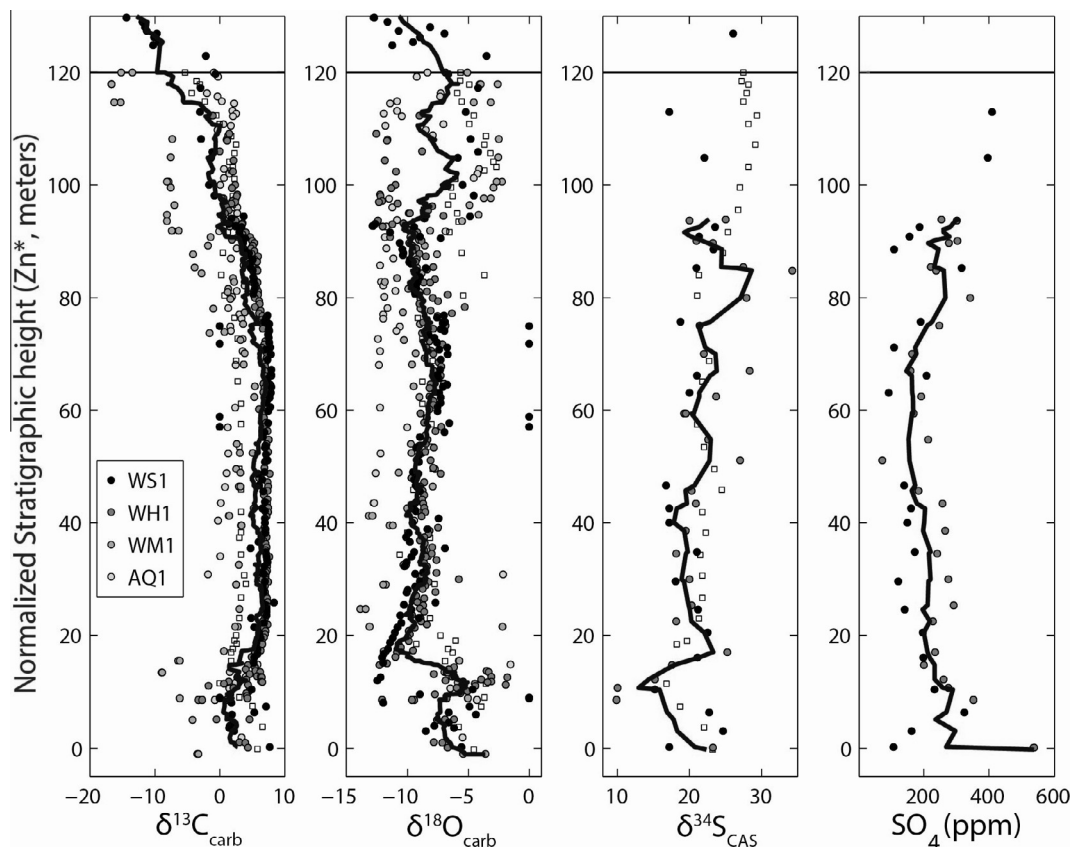
Fig. 3. Chemostratigaphic data from the Oman Mountain sections plotted against normalized stratigraphic height. The Khufai–Shuram formation boundary is shown in horizontal black lines. Heavy black lines indicate running averages of data from all areas. Data from Fike et al. (2006) are shown in open squares for C, O, and S isotopes but were not included for [SO$_4$] due to differing methodologies.

3‰ increase). After the sequence boundary, $\delta^{13}C$ values begin to decline (as in the Huqf); however, each section follows its own trajectory, with some sections producing remarkably depleted final excursion values. Oxygen isotope data are depleted ($\sim-10‰$) and are similar to the data from Fike et al. (2006).

Trends in $\delta^{34}S_{CAS}$ are also broadly similar between the Huqf and Oman Mountains, although absolute values are lower in the Oman Mountains. Lower sampling density and more condensed deposition precludes comparison to the excursions observed in the Huqf, but a general increase from 15 to >30‰ is observed. CAS concentrations are considerably lower in the Oman Mountains, ranging from ~100 to 500 ppm (Fig. 3). These values are consistent with most of the Huqf data but do not capture the large increase concurrent with isotopic enrichment.

6. EVALUATION OF TRENDS

6.1. Diagenetic effects

6.1.1. Geochemical predictions of diagenetic processes

Diagenetic processes can significantly alter the geochemical signals preserved in rocks and reset primary paleoenvironmental information in the process; however,

careful consideration of depositional and burial conditions as well as the relationships among different isotopic and elemental systems can help mitigate this risk. For example, cross plots between different proxies can facilitate comparisons of data to expected diagenetic trends (Fig. 4). This approach is commonly applied to the C and O isotope systems (e.g., Knauth and Kennedy, 2009) to illustrate the effects of meteoric and burial diagenesis. For the $\delta^{13}C$ and $\delta^{18}O$ isotope systems, meteoric diagenesis will drive carbonates to the lower left of Fig. 4A (blue arrow), whereas burial diagenesis will preferentially lower $\delta^{18}O$ (red arrow). Authigenic carbonate formation in the methanogenic zone of marine sediments would be expected to produce ^{13}C-depletion, strong $\delta^{34}S$ enrichment, and little change to $\delta^{18}O$ (orange arrows 4A and 4B). Also, covariation might be expected between $\delta^{18}O$ and [SO$_4$], as both are easily altered by meteoric diagenesis (Fike et al., 2006; Halverson and Hurtgen, 2007; Marenco et al., 2008; Gill et al., 2008). Specifically, positive correlation could suggest loss of CAS during meteoric diagenesis with an associated ^{16}O overprint on the carbonates— similar to Gill et al. (2008) (Fig. 4C, blue arrow). Meteoric alteration, however, should remove but not isotopically fractionate CAS (Gill et al., 2008)—thus limiting the diagenetic explanation for Fig. 4D.
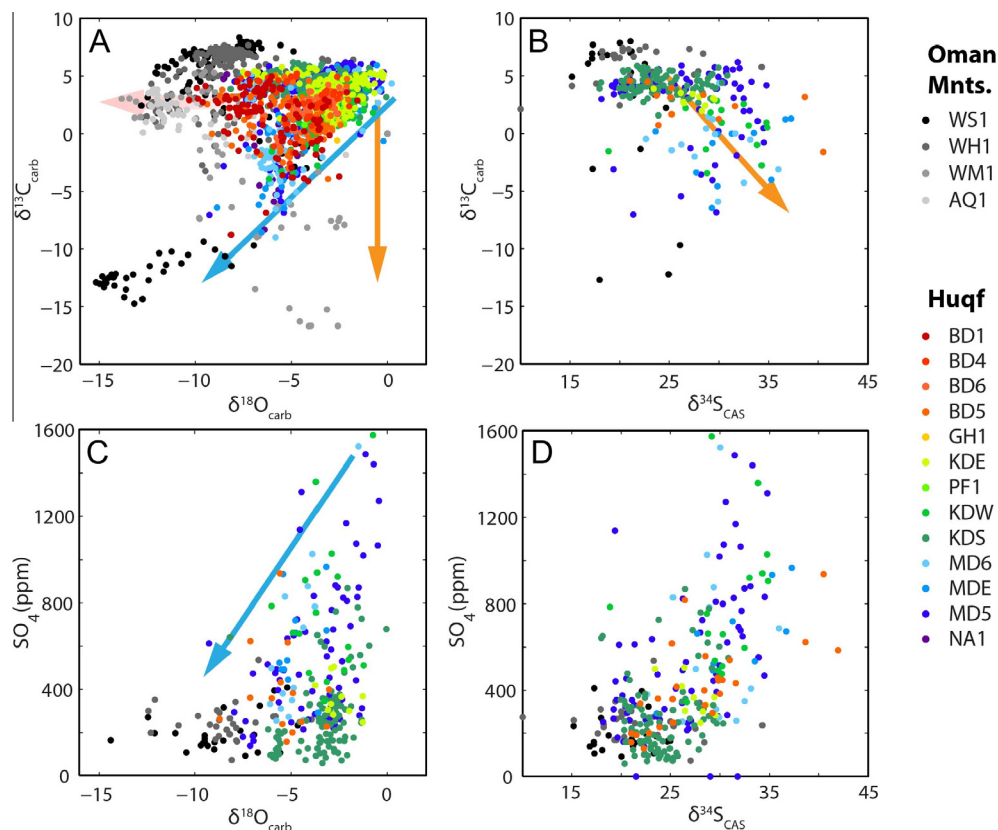
Fig. 4. Chemostratigraphic cross plots of selected data for both Huqf and Oman Mountains samples. Arrows indicate possible trajectories of diagenetic processes: meteoric diagenesis (blue), burial alteration (red), and authigenic carbonate precipitation (orange). (For interpretation of the references to colour in this figure legend, the reader is referred to the web version of this article.)

6.1.2. Evidence of diagenesis

The Huqf and Oman Mountain sections experienced very different depositional and burial histories with divergent potential for alteration of isotopic and compositional information. The Huqf Area is well preserved and has experienced only shallow burial and low tectonic overprints (Le Guerroue et al., 2006a; Allen, 2007). At least two phases of alteration occurred within this framework. The first was pervasive early dolomitization, although excellent retention of primary sedimentary fabrics suggests that dolomitization took place before or during lithification. Locally, severe recrystallization and deposition of coarse calcite spar in the outer- and middle-ramp facies occurred later, possibly associated with hydrothermal fluids (Osburn et al., 2014). In contrast, deep burial and tectonic overprinting has severely affected the integrity of isotopic signals in rocks from the Oman Mountains. Major tectonic events include pre-Permian burial, folding, and exhumation; deep burial associated with Cretaceous ophiolite abduction; and Neogene uplift of the Oman Mountains (Hanna and Nolan, 1989; Mann et al., 1990; Forbes et al., 2010). The resultant fabrics of the Khufai Formation range from well preserved to severely recrystallized, with evidence for ductile flow in carbonates and penetrative cleavage and phyllitic mica growth in siliciclastic sediments. Geochemical samples for this study were taken and processed to avoid secondary

fabrics, and emphasis was placed on the Huqf samples during interpretation due to their lower degree of alteration.

Evaluations of the cross plots show in Fig. 4 combined with our predictions and known geological history help identify altered samples and suggest generally excellent preservation of Huqf samples. Fig. 4A illustrates the distribution of carbon and oxygen isotope data showing that most samples populate the area between $\delta^{18}O$ of $-10\permil$ to $0\permil$ and $\delta^{13}C$ of $-1\permil$ to $+6\permil$. Despite careful sampling via microdrilling, isotopic evidence for alteration can be seen in the increased scatter and depletion of oxygen isotope data, particularly at Buah Dome (red and orange dots). This study area experienced a greater degree of alteration than the other Huqf exposures based on more widespread fabric destructive recrystallization, potentially because of fluid flow through its porous sand-dominated facies and its relative proximity to the Maradi Fault zone (Hanna and Nolan, 1989) (Fig. 1). Significant divergence from the main data cluster is seen for the Oman Mountains samples, which show enriched $\delta^{13}C$ and depleted $\delta^{18}O$ values, consistent with significant alteration during deep burial. Conversely, a trend of strong $\delta^{13}C$ depletion with minimal $\delta^{18}O$ change is defined by Huqf samples in the stratigraphic interval marked by the onset of the Shuram C-isotope excursion. The relationship between [CAS] and carbonate $\delta^{18}O$ (Fig. 4C) follows two trends based on

sample location: Oman Mountain samples display consistently low sulfate concentrations with a large range in $\delta^{18}O$, whereas Huqf samples show a large range in sulfate concentration but are restricted to a more narrow range in $\delta^{18}O$. As large ranges in [CAS] are preserved with little change in $\delta^{18}O$ for the Huqf dataset, we suggest that the [CAS] trends from these sections likely reflect primary trends in seawater but not necessarily absolute concentrations (compare Planavsky et al., 2012, and references therein; Paris et al., 2014).

Fig. 4D illustrates the relationship between [CAS] and $\delta^{34}S$ values. A positive correlation is observed that could be due to progressive evolution of seawater or mixing between normal Ediacaran seawater and an isotopically enriched and concentrated end-member. Such an isotopically enriched brine could not have been produced simply by the precipitation of gypsum due to the small positive fractionations associated with gypsum formation (Claypool et al., 1980) but could have been produced through bacterial sulfate reduction during evaporite formation as described by Fike (2007). However, evaporative brine formation should also alter $\delta^{18}O$, inconsistent with our previous observations. Broadly speaking, diagenetic processes do not appear to be the primary source of C and S isotope variability for the Khufai Formation. Where present, strong diagenetic signals can be identified based on fabric alteration or $\delta^{18}O$ variability and excluded from interpretation of primary environmental variables.

6.1.3. The potential role of diagenetic carbonate precipitation

Schrag et al. (2013) recently suggested that the Shuram carbon isotope excursion was produced through precipitation of ^{13}C-depleted authigenic carbonate within the excursion stratigraphy. Authigenic carbonate is defined in Schrag et al. (2013) as an *in situ* precipitated phase, where alkalinity production occurs through diagenetic reactions that would supplement primary marine DIC. The main carbon isotope decline in the Huqf occurs within a package of oolite followed by micritic carbonates, similar to other sections worldwide (Verdel et al., 2011; Loyd et al., 2012a,b). Our petrographic observations reveal that ooids retain primary radial-concentric fabrics (Osburn et al., 2014). Detailed drilling of ooid, cement, and micritic components in these units has shown no significant difference in carbon or oxygen isotopes in either the Khufai (this study) or Shuram formations (Bergmann, 2013). In addition, these high-energy facies likely contained very little primary organic matter due to winnowing and enhanced oxidation, leaving little to contribute to a depleted DIC pool. Furthermore, if our assertion is incorrect and there was sufficient organic matter to be remineralized by bacterial sulfate reduction in the sediments, we would expect the decline in $\delta^{13}C$ to be associated with strong $\delta^{34}S$ enrichment linked to bacterial sulfate reduction, exactly the opposite of the observed trend (4B, also see below). These observations support primary rather than secondary oolitic carbonate precipitation, thus challenging the model of Schrag et al. for a secondary origin for the Shuram excursion.

In contrast, isotopic heterogeneity in some sections of the Oman Mountains may result from authigenic carbonate input—particularly within the upper and lower transitional members where carbonates are restricted to irregular pockets and nodular beds surrounded by siliciclastic siltstone. In the lower transitional zone, large scatter with significantly depleted $\delta^{13}C$ values are observed along with relatively enriched $\delta^{18}O$ values, consistent with the variable inclusion of porewater DIC during lithification. In the upper transition zone, the Wadi Mistal section departs significantly from the others, displaying highly depleted $\delta^{13}C$ (down to $\sim-18‰$, orange arrow Fig. 4A). These extreme depletions follow the same trend as the Shuram Excursion observed in other sections, but the absolute values are particularly ^{13}C-depleted. We suggest that this relationship is consistent with a signature derived from a combination of ^{13}C-depleted marine DIC (following the trend of the Shuram excursion) and depleted DIC derived from organic matter remineralization during diagenesis. An individual stratum would inherit the marine DIC value at the time of its deposition then evolve to more depleted values via the addition of authigenic cements. In this manner the declining trend of the Shuram Excursion is preserved, albeit overprinted by authigenic precipitates. Notably, the Wadi Mistal section is stratigraphically condensed and organic-rich relative to the others—ideal conditions for the deposition of authigenic cements (Schrag et al., 2013). The concept of isotopically light authigenic carbonate precipitation is not new, having been noted in the carbonate concretion literature for decades (Curtis et al., 1972; Hudson, 1978; Mozley and Burns, 1993; Coleman, 1993); the critical point to the Shuram Excursion is that ^{13}C-depletion produced via this mechanism is unlikely to affect thick packages of carbonate and oolites and would be petrographically recognizable if it had.

6.2. Statistical evaluation of stratigraphic trends

A brief statistical treatment of the data is presented to evaluate the strength of stratigraphic trends and correlation among different proxies (Table 1). The Khufai Fm. was divided into six intervals to capture our three excursions, and statistical analyses were applied to evaluate the strength of isotopic trends spanning each. Analysis of $\delta^{13}C$ with stratigraphic height supports the presence of a subtle isotopic decline up to Zn* 300 m prior to a sharp decline marking the onset of the Shuram Excursion from Zn* 300 to 320 m (Table 1). Statistical analysis of sulfur isotope data with stratigraphic height strongly supports our identification of three excursions: increases in $\delta^{34}S_{CAS}$ that define Khufai 1 and Khufai 2, as well as a sharp $\delta^{34}S_{CAS}$ decrease in phase with the Shuram carbon isotope excursion. Concurrent CAS concentration changes are also supported by this analysis, displaying a strong increase with stratigraphic height between 150 and 300 m with a positive slope of 4.5 ppm/m. Additional, negatively sloping trends in [CAS] are also present between 75–100 and 300–320 m. Co-variation between C and S isotope systems is observed primarily in the upper Khufai Formation. The only robust trend in the lower Khufai formation is a strong negative correlation between the C and O isotope data from 0 to 25 m. In the upper Khufai Formation, negative correlation

Table 1
Correlation coefficients and statistical analysis.

Bin (Z_n^*)	Trends in stratigraphic height						Comparison between chemical systems							
	C		S		CAS		C vs. O		C vs. S		S vs. CAS		O vs. CAS	
	Slope	r	Slope	r	Slope	r	r	p	r	p	r	p	r	p
0–25	0.064	0.455	−0.109	−0.209	−9.090	−0.388	−0.93	**0.007**	−0.30	0.58	0.48	0.34	0.424	0.40
25–75	0.007	0.080	0.006	0.060	0.113	0.016	0.33	0.33	−0.11	0.75	−0.13	0.69	−0.042	0.90
75–100	−0.023	−0.076	0.229	0.267	13.642	0.475	0.083	0.88	0.19	0.72	0.25	0.63	0.031	0.95
100–150	−0.013	−0.151	−0.191	−0.679	−7.070	−0.466	−0.19	0.57	0.34	0.31	0.049	0.89	−0.16	0.65
150–300	−0.010	−0.277	0.067	0.704	4.475	0.539	0.13	0.50	−0.77	**<0.0001**	0.78	**<0.0001**	0.39	**0.002**
300–320	−0.296	−0.721	−0.419	−0.588	−10.706	−0.261	0.80	**0.006**	0.73	**0.018**	0.36	0.31	0.25	0.50
Total	−0.015	**−0.60**	**0.025**	0.52	1.4	**0.45**	0.42	**0.0003**	−0.29	**0.015**	0.71	**<0.0001**	0.20	0.10

Bold indicates statistical significance.

between $\delta^{13}C$ and $\delta^{34}S$ is observed between 150 and 300 m, positive correlation between $\delta^{13}C$ and $\delta^{18}O$ from 300 to 320 m, and positive correlation between $\delta^{34}S$ and [CAS] from 150 to 300 m. In total, this statistical treatment suggests that the trends observed for Khufai 2 are stronger than those of Khufai 1, although both are statistically robust.

6.3. Deconvolving facies-driven signals vs. stratigraphic trends

Sedimentary facies may differentially reflect diagenetic processes because of variations in permeability or depositional environment (i.e., mineralogy, grain size, organic carbon content). In addition, facies distributions often change systematically with stratigraphic architecture. This combination of effects complicates the distinction between local, facies-driven isotopic signals and global trends in ocean chemistry and thus must be addressed (Veizer et al., 1980). We analyzed isotopic trends in the context of both stratigraphic packages and facies groups to better understand the relative roles of each, if any, in this dataset (Fig. 5).

Broadly speaking, the chemostratigraphic data do not co-vary with facies, thereby validating our assertion that observed geochemical variability is mostly not a product of local environmental or lithologic control. However, several facies show distinctive trends that warrant discus-
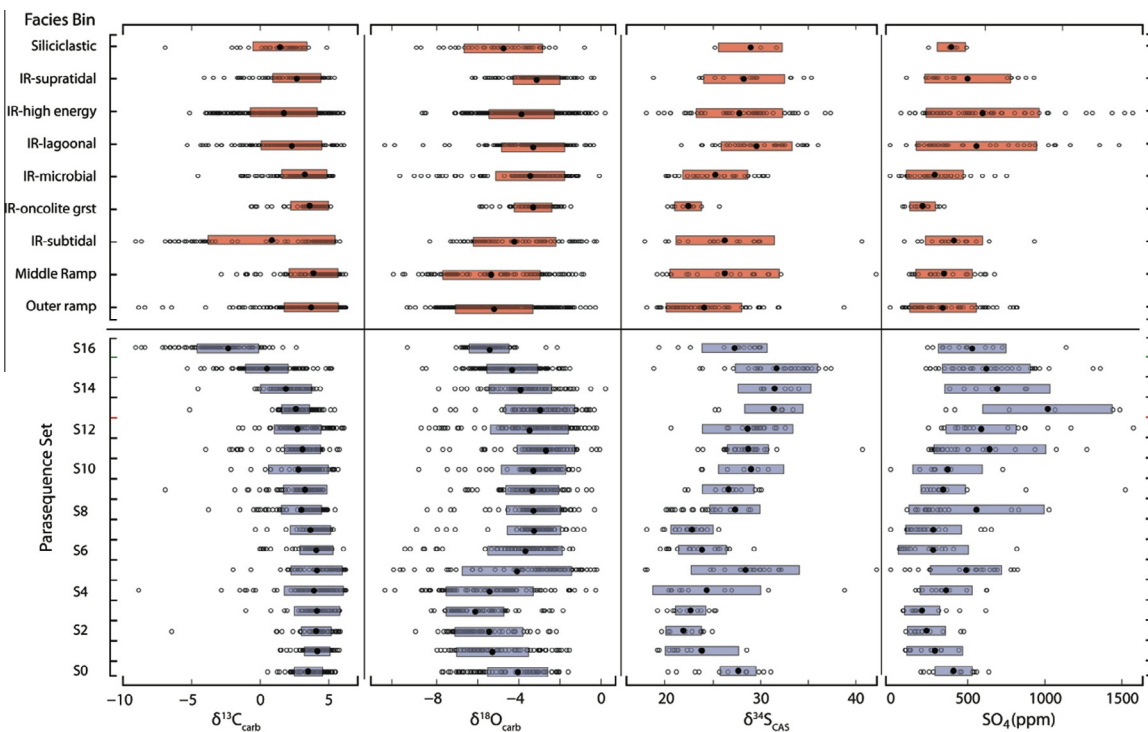

Fig. 5. A comparison of chemostratigraphic data binned by facies associations (upper panels) vs. stratigraphic package (lower panels). Individual data points are in open circles, where solid circles indicate the mean of each bin and the shaded bar shows two standard deviations.

sion. First, the inner-ramp subtidal facies association displays a bimodal $\delta^{13}C$ distribution extending to exceptionally low values. Further inspection reveals that the isotopically depleted facies only occurs at the very top of the formation during the decline into the Shuram Excursion. With this exception, the remainder of the facies association is isotopically similar to neighboring facies and the section average. Therefore, a temporally restricted facies yields the suggestion of environmental control when in fact it reflects a coincidence of stratigraphy. Similarly, the oncolite grainstone facies shows restricted ranges for all proxies, with unusually depleted $\delta^{34}S$ values and low [CAS]. As noted above, this facies also occupies a relatively narrow stratigraphic band that intersects a minimum in both sulfur isotope and [CAS] data between Khufai 1 and Khufai 2. In contrast, the inner ramp high energy and lagoonal facies associations show exceptionally large ranges and high values in [CAS]. These two associations represent very different environmental conditions, with the high-energy group reflecting open water deposition, and the lagoonal facies instead reflecting restricted conditions. If [CAS] reflected primarily local conditions, we would predict high [CAS] in the lagoonal and supratidal facies and low [CAS] in less restricted facies. We do see [CAS] enrichment of lagoonal facies, consistent with these predictions; however, the supratidal facies do not follow the predicted trend. High-energy facies also violate our local predictions, as very high [CAS] occurs in relatively open water environments. The lack of a coherent relationship between restriction and [CAS] suggests that stratigraphic/temporal controls, rather than local signals, control patterns in [CAS]. More specifically, facies-independent stratigraphic continuity suggests that the trends observed in our data reflect at least regional seawater evolution, and perhaps global trends, rather than local conditions.

7. DISCUSSION

Preceding the onset of the Shuram Excursion, the Khufai Formation displays consistently enriched $\delta^{13}C$, variable $\delta^{34}S$, and large changes in [CAS]. Here we will use mass balance-based modeling of the sulfur cycle to identify global environmental parameters that could have contributed to changes in the mass and $\delta^{34}S$ of the marine sulfate reservoir. First, we will explore possible mechanisms to account for trends within the sulfur system alone and then evaluate those options in light of the carbon isotope results.

7.1. Estimating timescale

In order to discuss rates of change, it is first necessary to establish a depositional timescale. This task is often difficult for Precambrian sedimentary sections, and the Khufai Formation is no exception due to the absence of direct geochronologic constraints (Bowring et al., 2007). The Huqf Supergroup is bounded below by the Hadash cap carbonate, with an inferred age of 635 Ma (Rieu et al., 2006; Bowring et al., 2007). There are no known dateable volcanic materials in the intervening Masirah Bay, Khufai, and Buah formations. The overlying Ara Group is con-

strained by an ash bed dated at 546.72 ± 0.21 in the A0 unit (Bowring et al., 2007). These brackets provide a maximum timescale of ~90 Ma for deposition of the Nafun Group. More specific estimates have placed the basal Shuram Formation at 560 Ma (Bowring et al., 2007) or linked the sequence boundary in the upper Khufai formation to the Gaskiers glacial at 580 Ma (Fike et al., 2006), thereby placing a maximum timeframe of Masirah Bay plus Khufai formation deposition at 75–55 Ma.

Given the lack of dated horizons, we instead estimate a depositional timescale using accumulation rates and cyclostratigraphy. Applying the conservative accumulation rates of 30 and 50 m/Ma for Precambrian carbonate platforms presented in Kah et al. (2004) yields estimates of 6.3–10.5 Ma for Khufai Formation deposition. Using accumulation rates calculated for the Paleoproterozoic Rocknest Formation from Grotzinger (1986) and Bowring and Grotzinger (1992) produces estimates of 5.6–7.6 Ma. Traditional timescale estimates for 4th and 5th order depositional sequences (Goldhammer et al., 1990) and the number of parasequences and parasequence sets published in Osburn et al. (2014) yield durations of 2–20 Ma. In addition, applying the depositional timescale estimates of Sadler (1981) complied for Phanerozoic carbonate platforms yields 3–30 Ma duration for the Khufai Formation deposition. The level of agreement between Phanerozoic (Goldhammer and Sadler) and Precambrian (Kah and Grotzinger) estimates is high given the fundamentally different mechanism of carbonate deposition prior to the evolution of skeletal carbonate producers. While there are significant differences, there is order-of-magnitude agreement between these methods, and for the remainder of this discussion we will assume a timescale of approximately 10 Ma and weigh the veracity of this assumption using sensitivity testing (see Supplementary Fig. A2).

7.2. Model parameters

We constructed a simple box model to represent the mass and isotopic components of the marine sulfate system. The governing equations used to drive these models are fundamentally based in mass balance—with the mass of the system representing a balance of input and output fluxes (Kump and Arthur, 1999; Kurtz, 2003). Our model was adapted from those of Kurtz (2003), Kah et al. (2004), and Halverson and Hurtgen (2007) and was constructed using the Stella® software package (ISEE Systems, 2011). The isotopic evolution of the sulfate reservoir of mass M_O is governed by the initial isotopic value of the sulfate reservoir (δ_O), isotopic value of the input fluxes (F_{in}: weathering [δ_W, F_w], hydrothermal [δ_{ht}, F_{ht}]), and the fractionation ($\Delta^{34}S$) associated with output fluxes (F_{out}: pyrite and sulfate burial [F_{py}, F_{sulf}]) following the equations provided previously by Kurtz (2003):

$$M_O = F_{ht} + F_W - F_{py} - F_{sulf} \qquad (1)$$

$$d\delta^{34}S/dt = (F_{in}(\delta_{in} - \delta_O) - F_{py}\Delta^{34}S)/M_O \qquad (2)$$

Buried sulfate was modeled as isotopically equivalent to seawater sulfate, despite the fractionation of up to $+1.7‰$ associated with evaporite formation (Claypool et al., 1980). This offset had very little effect on our results and

was excluded for simplicity. We applied this model in two ways. We first used our data as model bounds to invert for solutions of input parameters under different conditions. Second, we used a forward modeling approach to replicate the magnitude and shape of the two observed sulfur isotope excursions under both steady state and non-steady state conditions. Both of these approaches set bounds on the state of the marine sulfate system at the time of deposition.

7.3. The inverse approach

We will begin by using our data to constrain M_O, $\Delta^{34}S$, and F_{py} at different times. The rate of sulfur isotope change for marine sulfate is inversely proportional to the mass of the sulfate reservoir as it appears in Eq. (2). Slight rearrangement yields an expression for the mass of the sulfate reservoir:

$$M_O = \frac{(F_{in}(\delta_{in} - \delta_O) - F_{py}\Delta^{34}S)}{\frac{d\delta^{34}S}{dt}} \quad (3)$$

This relationship has been commonly applied to the Precambrian ocean to estimate the size of the marine sulfate reservoir (Hurtgen et al., 2002; Kah et al., 2004; Gellatly and Lyons, 2005; Halverson and Hurtgen, 2007; Loyd

et al., 2012a,b). Previous estimates for the Neoproterozoic ocean suggest an extremely small sulfate reservoir (Hurtgen et al., 2002; Kaufman et al., 2007; Canfield et al., 2010; Loyd et al., 2012a,b), with an increase in the latest Ediacaran (Fike et al., 2006; Halverson and Hurtgen, 2007).

Data from the Huqf were binned at 5 m intervals, and a running average for these data was taken as a conservative representation of isotopic change (Fig. 6A). An isotopic rate of change was calculated for each bin and analyzed using Eq. (3) (Fig. 6B) for F_{py} from 0.7 to 1.5 mol $\times 10^{18}$/ Ma, $\Delta^{34}S$ between 20‰ and 40‰, a F_{in} value of 1.5 mol $\times 10^{18}$/Ma, and δ_w of 8‰. No single pair of F_{py} and $\Delta^{34}S$ produced positive values for M_O for all stratigraphic intervals. Loyd et al. (2012a,b) noted that positive reservoir masses were only achieved for their data using $F_{py} = 1$, and they subsequently used this as a lower bound. This analysis constrains both the reservoir mass and the ranges of input parameters allowable in each stratigraphic bin (Fig. 6C and D).

The maximum possible M_O at each time step is shown in Fig. 6E. During periods of stable isotopic values, large M_O are permitted, whereas periods of rapid change require extremely small M_O. Particularly low sulfate concentrations are required at the end of the Khufai 1 (120–150 m) and at
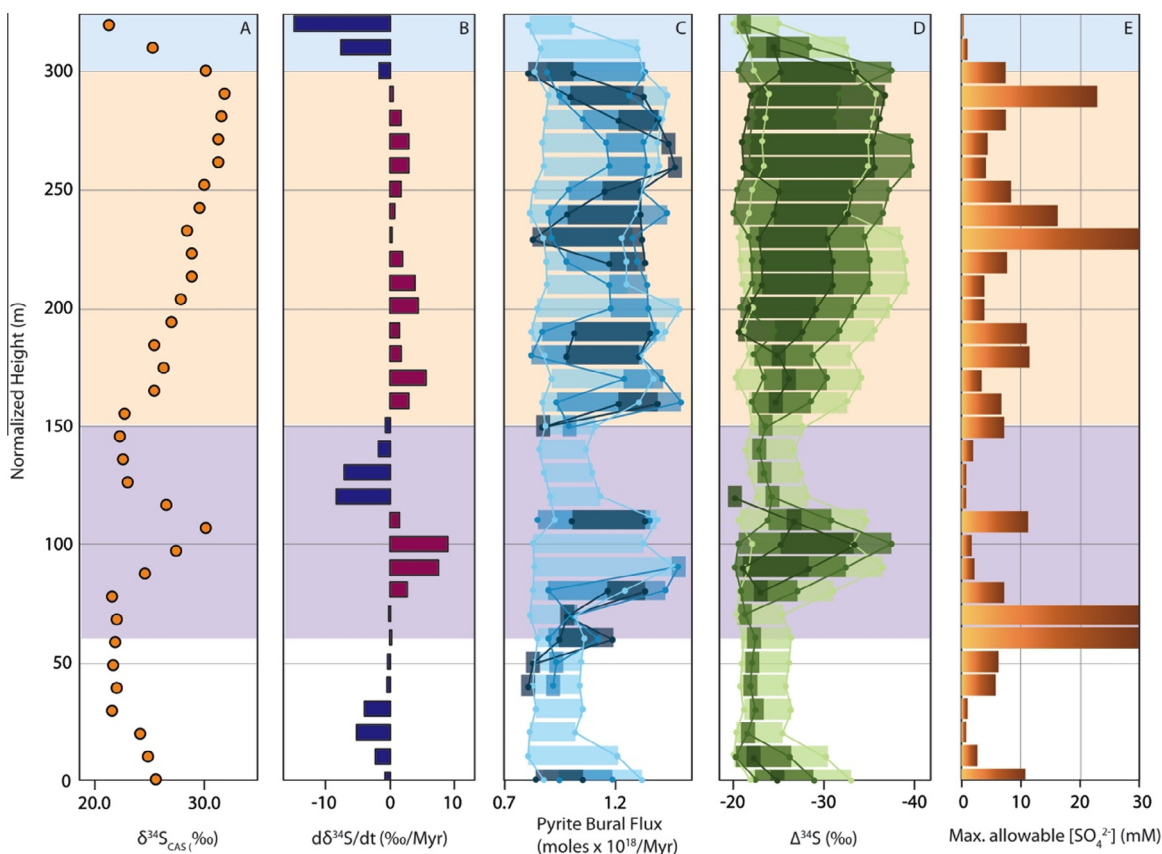

Fig. 6. Smoothed sulfur isotope data (A), rates of isotopic change for each bin (B), and the maximum allowable sulfate concentration calculated from reservoir size and rates of isotopic change (E). Pyrite burial flux (C) and fractionation (D) plots each show the results from calculations for $M_O = 0.288$, 4, and 8×10^{18} moles in the light, medium, and dark shaded tones, respectively. Khufai 1, 2, and Shuram onset are shown in the background purple, orange, and blue shaded boxes, respectively. (For interpretation of the references to colour in this figure legend, the reader is referred to the web version of this article.)

the onset of the Shuram Excursion (310–320 m). Ranges of F_{py} were used to calculate $\Delta^{34}S$ and vice versa for $M_O = 0.288$, 4, and 8×10^{18} moles (or 0.2 mM, 2.8 mM, and 5.6 mM concentrations of sulfate in seawater) and are plotted in Fig. 6C and D. Intervals of decreasing isotopic values generally allow only very small ranges for both F_{py} and $\Delta^{34}S$ and yield reasonable solutions only for the smallest reservoir mass, further supporting the idea of periodically very low sulfate concentrations throughout the Khufai Formation. Poor age control is a concern, but our conclusions do not change appreciably within the range discussed above. Significantly shorter timescales produce rapid rates of change that further restrict input

parameters and require increasingly small sulfate reservoir size (mostly <1 mM for excursion intervals), whereas longer depositional timescales are more accommodating to input parameter values and reservoir size (mostly >1 mM for excursion intervals). See Fig. A2 for sensitivity tests of Fig. 6 calculated at 5 Ma and 20 Ma depositional timescales.

7.4. Forward modeling of $\delta^{34}S$ excursions

We have implemented a forward modeling approach to evaluate causal mechanisms for the observed variations in $\delta^{34}S_{CAS}$. Khufai 1 shows a pulsed increase (22–28‰
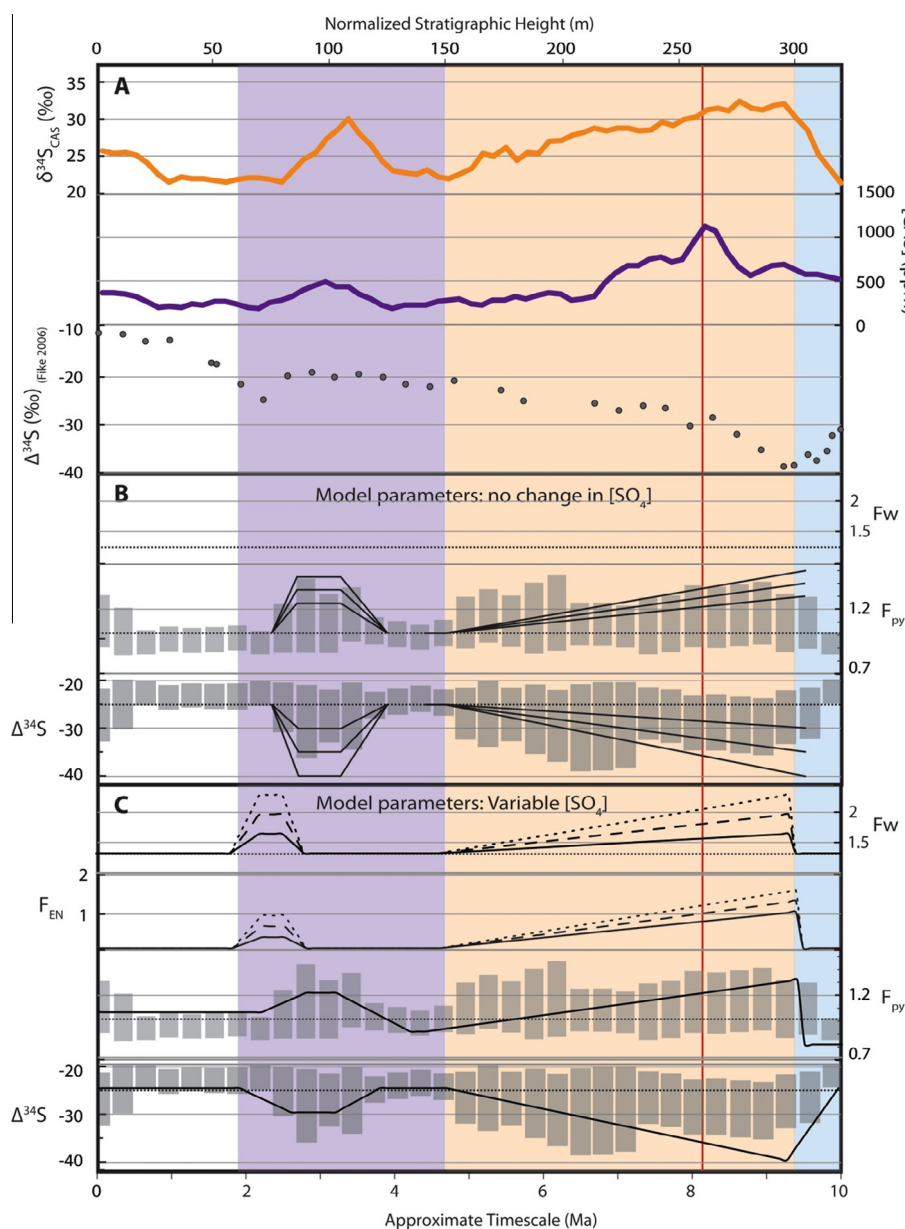

Fig. 7. Parameters for sulfur geochemical box model. (A) Smoothed sulfur isotope and CAS concentration data from this study with $\Delta^{34}S$ data from Fike et al. (2006) for comparison. (B) Input parameters for modeling with balanced input and output fluxes. Shaded bars indicate ranges allowed by calculations in Section 7.3 for $Mo = 0.288$ mol x 10^{18}. (C) Input parameters for modeling with increasing sulfate concentration. A constant $F_{sulf} = 0.45$ was used in these trials. Initialization conditions are equivalent to the values at time 0.

between 75 and 85 m) followed by relaxation to the baseline (20‰ by 145 m) over ~2 Ma. Khufai 2 is larger but slower, featuring a protracted rise in $\delta^{34}S$ from 20‰ to 35‰ between 155 and 310 m (~5 Ma). The Shuram $\delta^{34}S$ Excursion features a rapid decline from the highest observed $\delta^{34}S$ values to the lowest in ~20 m of stratigraphy. The climbing limbs of Khufai 1 and Khufai 2 are both accompanied by an increase in [CAS]. We attempt to replicate the basic trends and magnitudes of these excursions using modeling scenarios with either constant or increasing sulfate reservoir mass. The first attempt maintains balanced input and output fluxes and forces the isotopic system by transiently increasing either the ratio of pyrite-to-sulfate burial (f_{py}) or the fractionation associated with pyrite formation ($\Delta^{34}S$). The second approach allows the mass of the sulfate reservoir to increase through imbalances in input and output fluxes. Parameters used in both models are illustrated in Fig. 7B and C.

7.4.1. Balanced models

When input and output fluxes are balanced, isotopic changes are introduced either by changing pyrite burial flux (F_{py}) relative to sulfate burial and/or fractionation ($\Delta^{34}S$) or the isotopic composition of input fluxes. These variables have changed throughout Earth history and are implicated in other sulfur isotope excursions (Canfield, 2004; Fike and Grotzinger, 2010; Wu et al., 2010; Gill et al., 2011; Owens et al., 2013; Jones and Fike, 2013; Wu et al., 2015). Our calculations presented above indicate that changes in both fractionation and pyrite burial, as well as low sulfate concentration (<2.8 mM) are required to produce the

isotopic changes observed within the Khufai Formation. We investigated model response to increased F_{py} and $\Delta^{34}S$ for sulfate concentrations of 0.2, 0.6, and 1.2 mM with constant input fluxes (1.3 and 0.2×10^{18} moles/Ma, using δ_W and δ_{hy} of 6.5 and 3.5‰).

Fig. 8 illustrates the steady-state modeling output for Khufai 1 and Khufai 2 with increased fractionation (top) and pyrite burial (middle) or both (bottom). Increasing either F_{py} or $\Delta^{34}S$ (or a combination of both) can replicate the observed magnitude of Khufai 1 (~30‰), but individual variables were insufficient to replicate the magnitude of Khufai 2. Forcing $\Delta^{34}S$ of >30‰ for a 0.2 mM ocean or >40‰ for a 0.6 mM ocean resulted in sufficient magnitudes to replicate Khufai 1, as did an increase in F_{py} to 1.5×10^{18} moles/Ma. Khufai 2 is most easily replicated with $\Delta^{34}S$ increasing to >40‰ (see discussion below). In combination, increases in F_{py} and $\Delta^{34}S$ directly amplify one another, and thus most combined trials were successful below 1.2 mM sulfate. Increased reservoir mass mutes the rate and magnitude of isotope change in all cases and also suggests a mass <1.2 mM during Khufai 1 where modeled recovery occurs more slowly than the observed data.

We can evaluate the robustness of this approach by comparison to geologic evidence and to parameters calculated in Section 7.3. The difference between $\delta^{34}S_{CAS}$ and $\delta^{34}S_{pyr}$ ($\Delta^{34}S$) measured for the Khufai Formation by Fike et al. (2006) is plotted for reference on Fig. 7. These data suggest little increase in $\Delta^{34}S$ during Khufai 1 but a protracted increase to up to ~40‰ during Khufai 2. If fractionation remains constant during Khufai 1, pyrite burial fluxes approaching the magnitude of the combined input
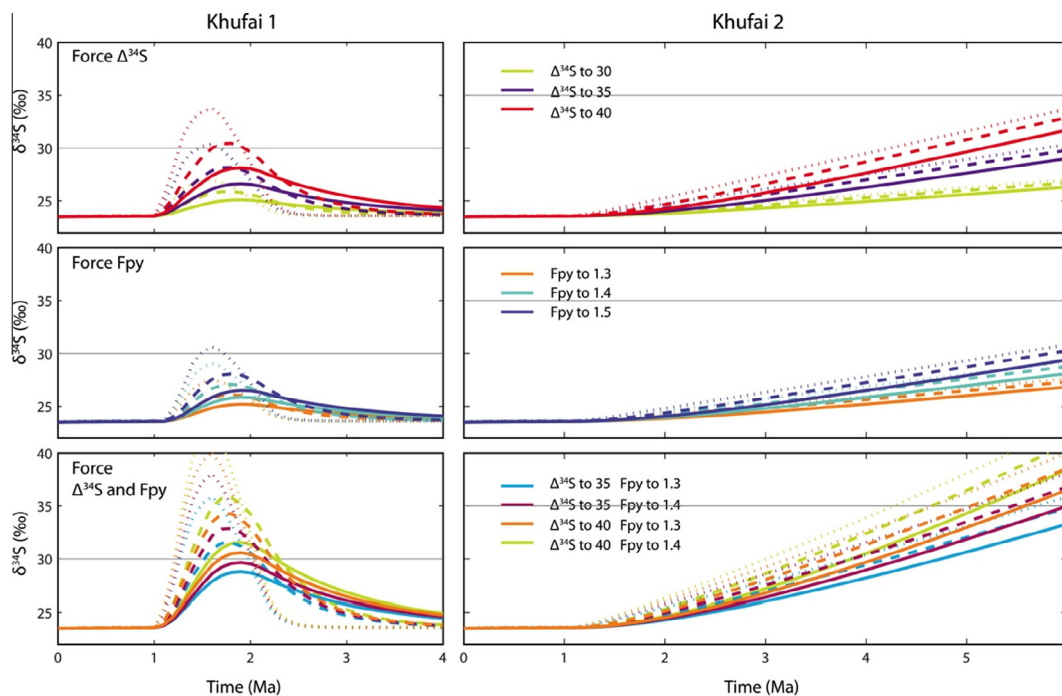

Fig. 8. Model output for Section 7.4.1. Khufai 1 and 2 are modeled separately and shown in the left and right hand panels, respectively. Each set of conditions is shown for marine sulfate concentration of 0.2, 0.6, and 1.2 mM illustrated in dotted, dashed, and solid lines, respectively.

fluxes are required. While the burial flux of pyrite was likely high at this time (Canfield, 2004; Maloof et al., 2010), we know that sulfate was also leaving the system globally, albeit in small amounts, as sedimentary gypsum (Osburn et al., 2014) and as CAS. The relatively high values of $\Delta^{34}S$ observed for during Khufai 2 constrain F_{py}—only matching observed $\delta^{34}S$ values at $F_{py} \geqslant 1.3 \times 10^{18}$ moles/Ma. Our model results suggest that $\Delta^{34}S$ increased during deposition of the Khufai Formation but illustrate that these changes alone are not sufficient to drive the observed $\delta^{34}S$ signatures, especial at >1 mM sulfate.

7.4.2. Increasing [SO₄]

The modeling results presented thus far are robust *only* if the concentration of sulfate in the ocean remained very low and constant. While direct interpretation of [CAS] as reflective of the coeval marine [SO₄] is uncertain, it is not without precedent (Planavsky et al., 2013), and the observed systematic changes in [CAS] within the Khufai Formation lack a clear alternative explanation (i.e., facies-based or diagenetic control). In recent experiments, Paris et al. (2014) find that foraminifera shells faithfully record the SO_4^{2-}/Ca^{2+} ratio of growth water and suggest that biogenic carbonate could be used to reconstruct [SO_4^{2-}] through geological time. While the validity of this approach in abiotic or microbial carbonates from the Neoproterozoic is not clear, successful application in a first-order sense to like carbonate components of modern biogenic carbonates is a hopeful first step. The global record of sulfate concentration through this time period is ambiguous and contradictory, but we can reasonably assume that the Ediacaran started with extremely low sulfate concentrations (Hurtgen et al., 2002; Halverson et al., 2005; Halverson et al., 2010) and, in Oman, ended in a large sulfate-rich evaporite deposit (Forbes et al., 2010), implying higher sulfate concentrations at least locally. In addition, elevated [CAS] are replicated in roughly correlative sections from Death Valley, N. Mexico, and South China, supporting the possibility of a global signal (Hurtgen et al., 2004; Kaufman et al., 2007; Loyd et al., 2012a,b). While our data certainly do not demand that [SO₄] increased during deposition of the Khufai Formation, such an increase is the most parsimonious explanation. To account for this option, we evaluate the model response to increases in the mass of the marine sulfate reservoir.

It is possible to change the modeled mass of the marine sulfate reservoir by reducing the magnitude of output relative to input fluxes—in this case, decreasing pyrite and/or sulfate burial fluxes. Decreasing pyrite burial is possible but would likely result in ^{34}S-depletion of marine sulfate, opposite of the observed trends. There is evidence for a very slight decrease in the burial fraction of pyrite (f_{py}) during this interval that is suggestive of at least local expanded ocean oxygenation (Canfield et al., 2007; Halverson and Hurtgen, 2007; Sahoo et al., 2012), but this decrease is minor compared to what is required to increase the mass of the sulfate reservoir significantly. Increasing sulfate mineral content and [CAS] of sedimentary rocks both globally and in the Khufai Formation during this time interval argue against a decrease in evaporite burial (Wright

et al., 1990; Strauss, 1993; Grotzinger et al., 2011). In this light, reduction of the output fluxes is not considered further.

Next we evaluate the possibility of $\delta^{34}S$ change via increasing F_W during excursion intervals without compensation in output fluxes (Fig. 9A–C). We applied pulsed fluxes of constant isotopic composition, either 6.5‰ or 12‰, to the model system. Instead of yielding positive isotope excursions at the intervals of interest, these trials produced negative excursions (9A, blue and green curves) because of the relatively depleted values of δ_W. Increasing the bulk δ_W value increases the equilibrium $\delta^{34}S$ value of the system but does not produce positive excursions, even when combined with the changes in F_{py} and $\Delta^{34}S$ suggested from the steady state modeling (9B, blue curves). These trials demonstrate that periodically increasing the weathering flux cannot account for the observed trends in $\delta^{34}S$ with a constant δ_W, regardless of the value.

In order to simultaneously account for increases in sulfate concentration and $\delta^{34}S$, we investigated scenarios where δ_W and F_W increase concurrently. While this manipulation alone produces only mild increases in $\delta^{34}S$ (Fig. 9A, orange curves), its impact, when acting in concert with previously applied F_{py} and $\Delta^{34}S$ increases, produces large changes in $\delta^{34}S$ (Fig. 9B, orange curves). In these models, modest isotope enrichment (12‰) at high flux (2.2×10^{18} moles/Ma) or more significant enrichment (16‰) at moderate flux (1.9×10^{18} moles/Ma) were sufficient to reproduce the trend and magnitude of observed $\delta^{34}S$ excursions. During these trials, the size of the marine sulfate reservoir increased from 0.2 to $2–4 \times 10^{18}$ moles (0.2 to 1.4–2.8 mM) in roughly 8 Ma.

Alternatively, the observed isotope and [CAS] increases can be reproduced by introducing an enriched input flux (F_{EN}) theoretically decoupled from F_W. Prescribed fluxes (F_{EN}) range from 1 to 1.6×10^{18} moles/Ma, with isotopic compositions (δ_{EN}) from 30‰ to 50‰, and were evaluated alone and in combination with F_{py} and $\Delta^{34}S$ increases (Fig. 9D–F). All trials that included this flux produced positive excursions that roughly approximate the trends seen in our data. F_{EN} greater than or equal to F_W with a δ_{EN} value of 50‰ is sufficient to explain our data alone, and, when applied in combination with F_{py} and $\Delta^{34}S$ increases (Fig. 9E), even our smallest modeled flux (1.0×10^{18} moles/Ma) can account for the observed trends. We will discuss potential sources of isotopically enriched sulfate in the following section.

7.5. Potential sources of enriched sulfate

In order to produce the observed S isotope excursions and parallel increase in marine sulfate concentration, our models require the addition of an enriched flux of sulfate. As weathering is the primary input of sulfur into our model, we will explore the possible isotopic variability of weathering inputs during the Neoproterozoic. We will also address possible inputs from other reservoirs such as restricted or stratified basins. The feasibility of these options is contingent on both the size of the possible reservoir and the plausibility of introducing anomalous sulfate into the marine system.
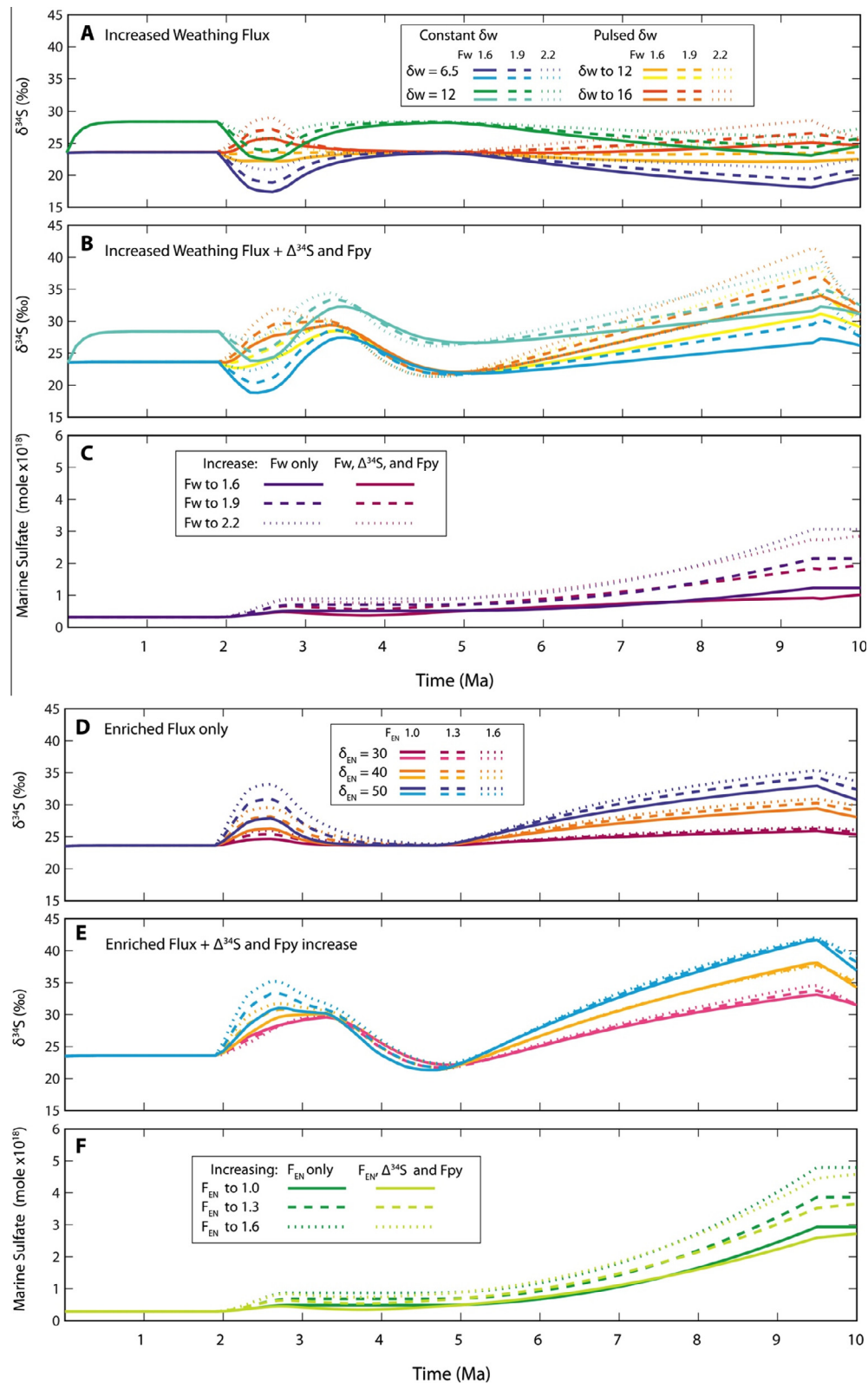
Fig. 9. (A–C) Model runs with excess weathering flux. (A) The resultant $\delta^{34}S$ from increasing F_W alone for various states of δw. (B) The combined effect of excess F_w with increasing fractionation and pyrite burial (trajectories shown in Fig. 7). (C) Mass of the marine sulfate reservoir for the various input conditions of F_W. (D–F) Model runs with the addition of an enriched flux of sulfate. (D) Resultant $\delta^{34}S$ for various enriched fluxes. (E) The combined effect of an enriched flux with increasing fractionation and pyrite burial (see Fig. 7). (F) The increase in the mass of the marine sulfate reservoir from varying inputs of F_{EN}.

The weathering flux of sulfate reflects the mass and isotopic signatures of dissolving sulfate (from gypsum/anhydrite) and oxidizing sulfides (principally pyrite). For modern systems, these processes release sulfate that is isotopically enriched and depleted, respectively (Claypool et al., 1980), although the isotopic variability and relative masses of these fluxes are poorly constrained during the Ediacaran. Using modern end member values, transiently increasing the ratio of sulfate-to-sulfide weathering produces a more positive δ_W. Data from the Khufai are most closely approximated using a pulse of δ_W of ~16‰, roughly equivalent to Phanerozoic estimates for the sulfate-derived flux alone (Kurtz, 2003). While this level of enrichment would be difficult to produce given modern reservoirs, Neoproterozoic $\delta^{34}S$ records of both sulfate and pyrite show enormous variability and include intervals of extreme isotopic enrichment for both (Ries et al., 2009; Halverson et al., 2010). Of particular interest to this discussion is the extreme isotopic enrichment of most pyrite deposited during the Cryogenian—ranging mostly from 10‰ to 50‰—and isotopic enrichments seen in both pyrite and CAS preceding the Shuram Excursion during the Ediacaran (Calver, 2000; Hurtgen et al., 2002; Kaufman et al., 2007; Xiao et al., 2012). If the rocks analyzed thus far are reflective of those weathered to sulfate during deposition of the Khufai Formation, a very enriched weathering flux could be produced. In addition, Wu et al. (2015) suggested increased inputs from evaporite weathering to account for higher positive $\delta^{34}S$ and $\Delta^{33}S$ within the overlying Ara group of Oman. Indeed, some combination of enhanced evaporite weathering and contributions from ^{34}S-enriched pyrite could account the trends observed in the Khufai Formation.

Another option for the enriched flux lies instead with a chemically isolated layer/basin within the ocean itself. The concept of a stratified Ediacaran ocean has been proposed previously (Rothman et al., 2003; Fike et al., 2006; Shen et al., 2008a; McFadden et al., 2008; Canfield et al., 2008; Ader et al., 2009), with support stemming from isotopic, sedimentological, and chemical arguments. Recently, Li et al. (2010) proposed a conceptual model wherein a sulfidic wedge is maintained, separating ferruginous deep waters from oxygenated surface waters. The sulfur isotope composition of the deep reservoir is presumed to have been driven to very enriched values through Rayleigh distillation during bacterial sulfate reduction with removal of the resulting isotopically light sulfide via pyrite formation (e.g., Rothman et al., 2003; Hurtgen et al., 2005; Fike et al., 2006; Kaufman et al., 2007; Shen et al., 2008a, 2010; McFadden et al., 2008; Grotzinger et al., 2011). However, the sulfate concentration of such seawater is required to be very low to maintain stratification (Shen et al., 2008a; Young, 2013), greatly reducing the likelihood that such a reservoir could supply significant quantities of sulfate to the surface ocean.

The global glaciations of the Neoproterozoic are relevant to this discussion of weathering fluxes and specifically the possibility of contributions from ^{34}S-enriched pyrite. The Ediacaran Period began just after the Marinoan Glaciation and contains the Gaskiers glacial event. Although likely smaller than the two main glacial episodes during the Cryogenian, the Gaskiers event was large and of at least regional significance. Glaciations are known to effect both ocean circulation and terrestrial weathering fluxes. If we adopt the rapid recycling model of Berner (2006) and the crustal memory effect of Reinhard et al. (2013), the youngest—that is, rocks highest in the underlying stratigraphy will be the most readily weathered. It follows from this relationship that preferential weathering of enriched sulfides and sulfates deposited before the Marinoan (and perhaps the pre-Gaskiers Ediacaran) is likely. During glacial events, erosional fluxes might be expected to be high, outpacing outpace burial fluxes and providing extensive substrates for chemical weathering post-glaciation. The advance and retreat of ice sheets might then produce pulsed weathering inputs, yielding the variability required by our models.

7.6. Constraints from the carbon isotopic record

We can further constrain the mechanisms of sulfur isotope change by comparison to the carbon isotope record. For the majority of deposition of the Khufai Formation, $\delta^{13}C$ values of carbonate are stable and enriched, hovering around 5‰. $\delta^{13}C$ of carbonate is basically invariant through Khufai 1 and decreases slightly through Khufai 2. At the onset of the Shuram Excursion, however, both $\delta^{13}C$ and $\delta^{34}S$ decrease rapidly. A mechanistic explanation for sulfur isotope change must be consistent with the carbon isotopic record.

In the steady-state scenario, increases in $\delta^{34}S$ result from increasing the fractionation associated with pyrite formation and the pyrite burial flux. Biological changes in $\Delta^{34}S$ should have no effect on the carbon isotope budget unless it is associated with large changes in productivity and subsequent carbon burial (see Fike and Grotzinger, 2008). However, pyrite and organic carbon burial are often associated because of the role of organic matter in driving bacterial sulfate reduction and because both pyrite and organic burial are favored by anoxic marine conditions. Thus, increasing F_{py} should be associated with a concurrent increase in carbon burial, resulting in increases in $\delta^{13}C_{carb}$ through mass balance relationships.

The signal of $\delta^{34}S$ and $\delta^{13}C$ linked to our postulated additional flux of sulfur varies considerably on where this flux originates. For instance, pyrite-rich deposits are commonly associated with weight % quantities of organic carbon as seen in several Mesozoic oceanic anoxic events (e.g., Gill et al., 2011; Owens et al., 2013) and as estimated for analogous Paleozoic events (Gill et al., 2012). Thus, pulsed weathering of organic carbon-rich, pyritic shales could then produce a ^{13}C-depleted flux of carbon and sulfate. Similarly, a flux originating from a DOC-rich deep ocean as postulated by Rothman et al. (2003) could be a source of ^{13}C-depleted carbon, although the characteristics of sulfur generated from such and oxidation are unknown. In contrast, weathering of an organic lean, but sulfur-bearing pool such as weathering of evaporite deposits, could produce sulfur isotope excursions independent of carbon isotope excursions.

Evaluating our excursions in this context places bounds on possible mechanisms. The invariance of carbon isotopes through Khufai 1 is consistent with either a change in $\Delta^{34}S$ (presumably not captured in Fike et al. (2006)) or a weathering input from an organic lean, isotopically heavy sulfur source, such as an evaporite deposit. The slight decline in $\delta^{13}C_{carb}$ during Khufai 2 is more permissive of inputs from either heavy sedimentary sulfide weathering or the deep ocean with oxidation of either sedimentary organic matter or marine DOC driving the C isotope record. The dramatic decline in both $\delta^{13}C_{carb}$ and $\delta^{34}S_{CAS}$ observed at the onset of the Shuram excursion necessitates large contemporaneous fluxes of isotopically light C and S, although previous authors have questioned the oxidant budget required to produce such fluxes (Bristow and Kennedy, 2008).

7.7. Implications to the Shuram Excursion

This study of the Khufai Formation places mechanistic constraints on the Shuram excursion. Here we show that decreasing $\delta^{13}C$ values at the excursion onset are associated with small decreases in $\delta^{18}O$ values and dramatic decreases in $\delta^{34}S_{CAS}$. Osburn et al. (2014) present sequence stratigraphic data from these same sections showing that the excursion onset significantly postdates the accommodation minimum and exposure surface within the upper Khufai Formation and instead occurs during flooding of the platform. These observations strongly challenge a meteoric alteration-based explanation of the Shuram Excursion. We do find evidence for the deposition of ^{13}C-depleted authigenic carbonates, but only in one unusual condensed section marked by carbonate concretions in the Oman Mountains. This signature is easily separated from the more prominent and widespread primary carbon isotope decline preserved in all other areas. Sulfur concentrations and isotope values are extremely variable prior to the Shuram Excursion, indicating a dynamic system with small reservoir size. Khufai 1 and 2 excursions can be attributed to changes in fractionation, pyrite burial, and the isotopic composition of the weathering flux. In contrast, at the onset of the Shuram Excursion sulfur isotopes drop by $\sim15\permil$ over the span of meters. This dramatic change in $\delta^{34}S$ is consistent with a large pulse of light sulfur linked to the source of light carbon that essentially overpowers the transient steady-state signal.

8. CONCLUSIONS

The Khufai Formation was deposited during a critical interval in Earth history and is uniquely positioned to document the environmental conditions prior to and during the initial Shuram isotopic excursion. We present a high-resolution record of sulfur and carbon isotopes through this interval, documenting a slow decline in carbon isotopes compared to rapid and large variability in the sulfur isotope record. CAS concentrations correspond generally to up-section increases in $\delta^{34}S$. Observed [CAS] scatter may reflect some level of secondary overprinting, and the primary absolute values could be altered, but the first-order trends are preserved. The complete decoupling from any facies/lithologic relationships and overarching sequence stratigraphic controls challenge simple explanations tied to diagenesis or local environmental drivers.

Our modeling results make predictions about both the general state of the sulfur system during the middle Ediacaran and changes at specific excursion intervals. Low sulfate concentrations (<1.2 mM) are required to permit the high rates of isotopic change observed during the middle Khufai Formation. This prediction is consistent with previous estimates for the size of the Ediacaran sulfate reservoir (Hurtgen et al., 2002; Kaufman et al., 2007; Loyd et al., 2012a,b), but our new high resolution data also suggests a significant increase in sulfate concentration during Khufai 2. Excursions in $\delta^{34}S$ can be explained by transient increases in either fractionation between sulfate and sulfide or the burial flux of pyrite (F_{py}), but these variables cannot account for our evidence for increases in sulfate concentration. If these increases in [CAS] reflect primary seawater trends, a flux of isotopically enriched sulfate is required to produce synchronous increases in $\delta^{34}S$ and [CAS], such as weathering of isotopically heavy pyrite or enhanced contributions from evaporites.

The onset of the Shuram carbon isotope excursion is captured in detail by our dataset, displaying exceptional preservation and strong relationships with the sulfur isotope system. We observe no evidence for increased meteoric diagenesis at the excursion interval and minimal contributions of authigenic carbonates. Our data support a primary origin for the Shuram Excursion that is temporally and perhaps mechanistically linked to ^{34}S-depletion of sulfate. An extreme weathering and oxidation event or massive volcanic/hydrothermal input could potentially explain this link.

APPENDIX A

See Table A1.

Table A1
Section locations and data.

Section name	Abbr.	Lat[a]	Long	Thickness (m)[b]	C/O	CAS[c]
Oman Mountains						
Wadi Sahtan 1	WS1	23.22366	57.31208	204	*	*
Wadi Hajir 1	WH1	23.20498	57.5592	181	*	*
Wadi Bani Awf	WBA	23.24078	57.40588	30.4*	*	
Al Aqor Village 1	AQ1	23.07361	57.66517	76.7	*	
Wadi Mistal 1	WM1	23.12724	57.75148	54	*	
Huqf						
Buah Dome 1	BD1	20.38214	57.68652	272	*	
Buah Dome 8	BD8	20.38358	57.69339	303.5	*	
Buah Dome 6	BD6	20.35387	57.68817	91*	*	
Buah Dome 5	BD5	20.35182	57.6862	307.8	*	*
Goose Chase 1	GH1	20.33477	57.78247	14.7*	*	
Khufai Dome East	KDE	20.23195	57.69993	319.1*	*	(local)
Khufai Dome South	KDS	20.13538	57.6405	307.8*	*	*
Khufai Dome West	KDW	20.11736	57.59718	131.8*	*	(local)
Post-Fault 1	PF1	20.13799	57.58743	28.8*	*	
Mukhaibah Dome 6	MD6	19.98238	57.71587	260.9*	*	(local)
Mukhaibah Dome East	MDE	19.96842	57.71682	293.4*	*	(local)
Mukhaibah Dome 5	MD5	19.94093	57.70551	312.1	*	*
Nafun 1	NA1	19.87315	57.69944	19.8*	*	

[a] WGS84 coordinate system.
[b] (*) indicates that the section is incomplete.
[c] Local indicates that the whole stratigraphic section was not analyzed.

APPENDIX B. SUPPLEMENTARY DATA

Supplementary data associated with this article can be found, in the online version, at http://dx.doi.org/10.1016/j.gca.2015.07.039.

REFERENCES

Ader M., Macouin M., Trindade R. I. F., Hadrien M. H., Yang Z., Sun Z. and Besse J. (2009) A multilayered water column in the Ediacaran Yangtze platform? Insights from carbonate and organic matter paired δ^{13}C. *Earth Planet. Sci. Lett.* **288**, 213–227.

Allen P. A. (2007) The Huqf Supergroup of Oman: basin development and context for Neoproterozoic glaciation. *Earth Sci. Rev.* **84**, 139–185.

Amthor J. E., Grotzinger J. P., Schroder S., Bowring S. A., Ramezani J., Martin M. W. and Matter A. (2003) Extinction of Cloudina and Namacalathus at the Precambrian-Cambrian boundary in Oman. *Geology* **31**, 431–434.

Bartley J. K. and Kah L. C. (2004) Marine carbon reservoir, C-org-C-carb coupling, and the evolution of the Proterozoic carbon cycle. *Geology* **32**, 129–132.

Berner R. A. (2006) GEOCARBSULF: a combined model for Phanerozoic atmospheric O2 and CO2. *Geochim. Cosmochim. Acta* **70**, 5653–5664.

Bergmann K. D., Zentmyer R. A. and Fischer W. W. (2011) The stratigraphic expression of a large negative carbon isotope excursion from the Ediacaran Johnnie Formation, Death Valley. *Precambr. Res.* **188**, 45–56.

Bergmann, K. D. (2013) Constraints on the carbon cycle and climate during the early evolution of animals. Dissertaion (Ph. D.), California Institute of Technology. <http://resolver.caltech.edu/CaltechTHESIS:06102013-045943358>.

Bowring S. A. and Grotzinger J. P. (1992) Implications of new chronostratigraphy for tectonic evolution of Wopmay Orogen, Northwest Canadian Shield. *Am. J. Sci.* **292**, 1–20.

Bowring S. A., Grotzinger J. P., Condon D. J., Ramezani J., Newall M. J. and Allen P. A. (2007) Geochronologic constraints on the chronostratigraphic framework of the Neoproterozoic Huqf Supergroup, Sultanate of Oman. *Am. J. Sci.* **307**, 1097–1145.

Brennan S. T., Lowenstein T. K. and Horita J. (2004) Seawater chemistry and the advent of biocalcification. *Geology* **32**, 473–476.

Bristow T. F. and Kennedy M. J. (2008) Carbon isotope excursions and the oxidant budget of the Ediacaran atmosphere and ocean. *Geology* **36**, 863.

Burdett J., Arthur M. and Richardson M. (1989) A Neogene seawater sulfur isotope age curve from calcareous pelagic microfossils. *Earth Planet. Sci. Lett.* **94**, 189–198.

Burns S. J. and Matter A. (1993) Carbon isotopic record of the latest Proterozoic from Oman. *Eclogae Geol. Helv.* **86**, 595–607.

Calver C. (2000) Isotope stratigraphy of the Ediacarian (Neoproterozoic III) of the Adelaide Rift Complex, Australia, and the overprint of water column stratification. *Precambr. Res.* **100**, 121–150.

Canfield D. E. (2004) The evolution of the Earth surface sulfur reservoir. *Am. J. Sci.* **304**, 839–861.

Canfield D. E., Farquhar J. and Zerkle A. L. (2010) High isotope fractionations during sulfate reduction in a low-sulfate euxinic ocean analog. *Geology* **38**, 415–418.

Canfield D. E., Poulton S. W. and Narbonne G. M. (2007) Late-Neoproterozoic deep-ocean oxygenation and the rise of animal life. *Science* **315**, 92–95.

Canfield D. E., Poulton S. W., Knoll A. H., Narbonne G. M., Ross G., Goldberg T. and Strauss H. (2008) Ferruginous conditions dominated later Neoproterozoic deep-water chemistry. *Science* **321**, 949–952.

Claypool G. E., Holser W. T., Kaplan I. R., Sakai H. and Zak I. (1980) The age curves of sulfur and oxygen isotopes in marine sulfate and their mutual interpretation. *Chem. Geol.* **28**, 199–260.

Coleman M. L. (1993) Microbial processes – controls on the shape and composition of carbonate concretions. *Mar. Geol.* **113**, 127–140.

Corsetti F. A. and Kaufman A. J. (2003) Stratigraphic investigations of carbon isotope anomalies and Neoproterozoic ice ages in Death Valley, California. *Geol. Soc. Am. Bull.* **115**, 916–932.

Curtis C. D., Petrowski C. and Oertel G. (1972) Stable carbon isotope ratios within carbonate concretions: a clue to place and time of formation. *Nature* **235**, 98–100.

Derry L. (2010) A burial diagenesis origin for the Ediacaran Shuram-Wonoka carbon isotope anomaly. *Earth Planet. Sci. Lett.* **294**, 152.

Erwin D. H., Laflamme M., Tweedt S. M., Sperling E. A., Pisani D. and Peterson K. J. (2011) The Cambrian conundrum: early divergence and later ecological success in the early history of animals. *Science* **334**, 1091–1097.

Fike D. (2007) *Carbon and Sulfur Isotopic Constraints on Ediacaran Biogeochemical Processes, Huqf Supergroup, Sultanate of Oman*. Massachusetts Institute of Technology.

Fike D. A. and Grotzinger J. P. (2008) A paired sulfate–pyrite $\delta^{34}S$ approach to understanding the evolution of the Ediacaran–Cambrian sulfur cycle. *Geochim. Cosmochim. Acta* **72**, 2636–2648.

Fike D. A. and Grotzinger J. P. (2010) A $^{34}S_{SO4}$ approach to reconstructing biogenic pyrite burial in carbonate-evaporite basins: an example from the Ara Group, Sultanate of Oman. *Geology* **38**, 371–374.

Fike D. A., Grotzinger J. P., Pratt L. M. and Summons R. E. (2006) Oxidation of the Ediacaran Ocean. *Nature* **444**, 744–747.

Forbes G., Jansen H. and Schreurs J. (2010) *Lexicon of Oman Subsurface Stratigraphy*. GeoArabia Special Publication, Manams, Bahrain.

Garrels R. M. and Lerman A. (1981) Phanerozoic cycles of sedimentary carbon and sulfur. *Proc. Natl. Acad. Sci. U.S.A.* **78**, 4652–4656.

Gellatly A. M. and Lyons T. W. (2005) Trace sulfate in mid-Proterozoic carbonates and the sulfur isotope record of biospheric evolution. *Geochim. Cosmochim. Acta* **69**, 3813–3829.

Gill B. C., Lyons T. W. and Frank T. D. (2008) Behavior of carbonate-associated sulfate during meteoric diagenesis and implications for the sulfur isotope paleoproxy. *Geochim. Cosmochim. Acta* **72**, 4699–4711.

Gill B. C., Lyons T. W. and Jenkyns H. C. (2011) A global perturbation to the sulfur cycle during the Toarcian Oceanic Anoxic Event. *Earth Planet. Sci. Lett.* **312**, 484–496.

Gill B. C., Lyons T. W., Young S. A., Kump L. R., Knoll A. H. and Saltzman M. R. (2012) Geochemical evidence for widespread euxinia in the Later Cambrian ocean. *Nature* **469**, 80–83.

Goldhammer R. K., Dunn P. A. and Hardie L. A. (1990) Depositional styles, composite sea-level changes, cycle stacking patterns, and the hierarchy of stratigraphic forcing: examples from Alpine Triassic platform carbonates. *GSA Bull.* **102**, 535–562.

Grotzinger J. P. (1986) Cyclicity and paleoenvironmental dynamics, Rocknest platform, northwest Canada. *GSA Bull.* **97**, 1208–1231.

Grotzinger J. P., Fike D. A. and Fischer W. W. (2011) Enigmatic origin of the largest-known carbon isotope excursion in Earth's history. *Nat. Geosci.* **4**, 285–292.

Halverson G. and Hurtgen M. T. (2007) Ediacaran growth of the marine sulfate reservoir. *Earth Planet. Sci. Lett.* **263**, 32–44.

Halverson G. P., Hoffman P. F., Schrag D. P., Maloof A. C. and Rice A. H. N. (2005) Toward a Neoproterozoic composite carbon-isotope record. *Geol. Soc. Am. Bull.* **117**, 1181.

Halverson G. P., Wade B. P., Hurtgen M. T. and Barovich K. M. (2010) Neoproterozoic chemostratigraphy. *Precambr. Res.* **182**, 337–350.

Halverson G. P. and Shields-Zhou G. (2011) *Chapter 4: Chemostratigraphy and the Neoproterozoic Glaciations*. Geological Society, London, Memoirs 36, pp. 51–66.

Hanna S. and Nolan S. (1989) The maradi fault zone – evidence of late neogene tectonics in the Oman mountains. *J. Geol. Soc. Lond.* **146**, 867–871.

Hoffman P. F., Kaufman A. J., Halverson G. P. and Schrag D. P. (1998) A Neoproterozoic snowball earth. *Science* **281**, 1342–1346.

Hudson J. D. (1978) Concretions, isotopes, and the diagenetic history of the Oxford Clay (Jurassic) of central England. *Sedimentology* **25**, 339–370.

Hurtgen M. T., Arthur M. A. and Halverson G. P. (2005) Neoproterozoic sulfur isotopes, the evolution of microbial sulfur species, and the burial efficiency of sulfide as sedimentary pyrite. *Geology* **33**, 41.

Hurtgen M. T., Arthur M. A. and Prave A. R. (2004) The sulfur isotope composition of carbonate-associated sulfate in Mesoproterozoic to Neoproterozoic carbonates from Death Valley, California. *Geol. Soc. Am. Special Paper* **379**, 177–194.

Hurtgen, Arthur, Suits and Kaufman (2002) The sulfur isotopic composition of Neoproterozoic seawater sulfate: implications for a snowball Earth? *Earth Planet. Sci. Lett.* **203**, 17–17.

Johnston D. T., Poulton S. W., Goldberg T., Sergeev V. N., Podkovyrov V., Vorob'eva N. G., Bekker A. and Knoll A. H. (2012) Late Ediacaran redox stability and metazoan evolution. *Earth Planet. Sci. Lett.* **335**, 25–35.

Jones D. S. and Fike D. A. (2013) Dynamic sulfur and carbon cycling through the end-Ordovician extinction revealed by paired sulfate–pyrite $\delta^{34}S$. *Earth Planet. Sci. Lett.* **363**, 144–155.

Kah L. C., Lyons T. W. and Frank T. D. (2004) Low marine sulphate and protracted oxygenation of the Proterozoic biosphere. *Nature* **431**, 834–838.

Kampschulte A. and Strauss H. (2004) The sulfur isotopic evolution of Phanerozoic seawater based on the analysis of structurally substituted sulfate in carbonates. *Chem. Geol.* **204**, 255–286.

Kaufman A. J., Knoll A. H. and Narbonne G. M. (1997) Isotopes, ice ages, and terminal Proterozoic earth history. *Proc. Natl. Acad. Sci. U.S.A.* **94**, 6600–6605.

Kaufman A. J., Corsetti F. A. and Varni M. A. (2007) The effect of rising atmospheric oxygen on carbon and sulfur isotope anomalies in the Neoproterozoic Johnnie Formation, Death Valley, USA. *Chem. Geol.* **237**, 47–63.

Knauth L. and Kennedy M. (2009) The late Precambrian greening of the Earth. *Nature* **460**, 728–732.

Kump L. R. and Arthur M. A. (1999) Interpreting carbon-isotope excursions: carbonates and organic matter. *Chem. Geol.* **161**, 181–198.

Kurtz A. C. (2003) Early Cenozoic decoupling of the global carbon and sulfur cycles. *Paleoceanography* **18**, 1–14.

Le Guerroue E., Allen P. A. and Cozzi A. (2006a) Chemostratigraphic and sedimentological framework of the largest negative carbon isotopic excursion in Earth history: The Neoproterozoic Shuram Formation (Nafun Group, Oman). *Precambr. Res.* **146**, 68–92.

Le Guerroue E., Allen P. A., Cozzi A., Etienne J. L. and Fanning M. (2006b) 50 Myr recovery from the largest negative $\delta^{13}C$ excursion in the Ediacaran ocean. *Terra Nova* **18**, 147–153.

Le Guerroue E. (2010) Duration and synchroneity of the largest negative carbon isotope excursion on Earth: The Shuram/Wonoka anomaly. *Comptes Rendus Geosci* **342**, 204–214.

Lenton T. M., Boyle R. A., Poulton S. W., Shields-Zhou G. A. and Butterfield N. J. (2014) Co-evolution of eukaryotes and ocean oxygenation in the Neoproterozoic era. *Nat. Geosci.* **7**, 257–265.

Li C. C., Love G. D. G., Lyons T. W. T., Fike D. A. A., Sessions A. L. A. and Chu X. X. (2010) A stratified redox model for the Ediacaran ocean. *Science* **328**, 80–83.

Love G. D., Grosjean E., Stalvies C., Fike D. A., Grotzinger J. P., Bradley A. S., Kelly A. E., Bhatia M., Meredith W., Snape C. E., Bowring S. A., Condon D. J. and Summons R. E. (2009) Fossil steroids record the appearance of Demospongiae during the Cryogenian period. *Nature* **457**, 718–721.

Loyd S. J., Marenco P. J., Hagadorn J. W., Lyons T. W., Kaufman A. J., Sour-Tovar F. and Corsetti F. A. (2012a) Local d^{34}S variability in ∼580 Ma carbonates of northwestern Mexico and the Neoproterozoic marine sulfate reservoir. *Precambr. Res.* **224**, 551–569.

Loyd S. J., Marenco P. J., Hagadorn J. W., Lyons T. W., Kaufman A. J., Sour-Tovar F. and Corsetti F. A. (2012b) Sustained low marine sulfate concentrations from the Neoproterozoic to the Cambrian Insights from carbonates of northwestern Mexico and eastern California. *Earth Planet. Sci. Lett.* **339–340**, 79–94.

Lyons T. W., Reinhard C. T., Love G. D. and Xiao S. (2012) Geobiology of the Proterozoic Eon. In *Fundementals of Geobiology* (eds. A. H. Knoll, D. E. Canfield and K. O. Konhauser). Blackwell Science, pp. 371–401.

Lyons T. W., Reinhard C. T. and Planavsky N. J. (2014) The rise of oxygen in Earth's early ocean and atmosphere. *Nature* **506**, 307–315.

Macdonald F. A., Schmitz M. D., Crowley J. L., Roots C. F., Jones D. S., Maloof A. C., Strauss J. V., Cohen P. A., Johnston D. T. and Schrag D. P. (2010) Calibrating the Cryogenian. *Science* **327**, 1241–1243.

Maloof A. C., Porter S. M., Moore J. L., Dudas F. O., Bowring S. A., Higgins J. A., Fike D. A. and Eddy M. P. (2010) The earliest Cambrian record of animals and ocean geochemical change. *Geol. Soc. Am. Bull.* **122**, 1731–1774.

Mann A., Hanna S., Robertson A., Searle M. and Ries A. (1990) The tectonic evolution of pre-Permian rocks, Central and Southeastern Oman Mountains. *Geol. Tecton. Oman Region*, 307–325.

Marenco P. J., Corsetti F. A., Kaufman A. J. and Bottjer D. J. (2008) Environmental and diagenetic variations in carbonate associated sulfate: an investigation of CAS in the Lower Triassic of the western USA. *Geochim. Cosmochim. Acta* **72**, 1570–1582.

McFadden K. A., Huang J., Chu X., Jiang G., Kaufman A. J., Zhou C., Yuan X. and Xiao S. (2008) Pulsed oxidation and biological evolution in the Ediacaran Doushantuo Formation. *PNAS* **105**, 3197–3202.

Melezhik V. A., Pokrovsky B. G., Fallick A. E., Kuznetsov A. B. and Bujakaite M. I. (2009) Constraints on 87Sr/86Sr of Late Ediacaran seawater: insight from Siberian high-Sr limestones. *J. Geol. Soc. London* **166**, 183–191.

Mozley P. S. and Burns S. J. (1993) Oxygen and carbon isotopic composition of marine carbonate concretions – an overview. *J. Sediment. Petrol.* **63**, 73–83.

Narbonne G. M. (2005) THE EDIACARA BIOTA: Neoproterozoic origin of animals and their ecosystems. *Annu. Rev. Earth Planet. Sci.* **33**, 421–442.

Narbonne G. M., Kaufman A. J. and Knoll A. H. (1994) Integrated chemostratigraphy and biostratigraphy of the Windermere Supergroup, northwestern Canada – Implications for Neoproterozoic correlations and the early evolution of animals. *Geol. Soc. Am. Bull.* **106**, 1281–1292.

Osburn M. O., Grotzinger J. and Bergmann K. (2014) Facies, stratigraphy, and evolution of a middle Ediacaran carbonate ramp: Khufai Formation, Sultanate of Oman. *AAPG Bull.* **98**, 1631–1667.

Owens J. D., Gill B. C., Jenkyns H. C., Bates S. M., Severmann S., Kuypers M. M., Woodfine R. G. and Lyons T. W. (2013) Sulfur isotopes track the global extent and dynamics of euxinia during Cretaceous Oceanic Anoxic Event 2. *Proc. Natl. Acad. Sci. U.S.A.* **110**, 18407–18412.

Paris G., Fehrenbacher J. S., Sessions A. L., Spero H. J. and Adkins J. F. (2014) Experimental determination of carbonate-associated sulfate δ^{34}S in planktonic foraminifera shells. *Geochem. Geophys. Geosyst.* **15**, 1452–1461.

Paytan A., Kastner M., Campbell D. and Thiemens M. (1998) Sulfur isotopic composition of Cenozoic seawater sulfate. *Science* **282**, 1459–1462.

Paytan A., Kastner M., Campbell D. and Thiemens M. H. (2004) Seawater sulfur isotope fluctuations in the cretaceous. *Science* **304**, 1663–1665.

Planavsky N. J. N., Bekker A. A., Hofmann A. A., Owens J. D. J. and Lyons T. W. T. (2012) Sulfur record of rising and falling marine oxygen and sulfate levels during the Lomagundi event. *Proc. Natl. Acad. Sci. U.S.A.* **109**, 18300–18305.

Prave A. R., Fallick A. E., Thomas C. W. and Graham C. M. (2009) A composite C-isotope profile for the Neoproterozoic Dalradian Supergroup of Scotland and Ireland. *J. Geol. Soc. Lond.* **166**, 845–857.

Reinhard C. T., Planavsky N. J. and Lyons T. W. (2013) Long-term sedimentary recycling of rare sulphur isotope anomalies. *Nature* **497**, 100–103.

Ries J. B., Fike D. A., Pratt L. M., Lyons T. W. and Grotzinger J. P. (2009) Superheavy pyrite (34Spyr > 34SCAS) in the terminal Proterozoic Nama Group, southern Namibia: a consequence of low seawater sulfate at the dawn of animal life. *Geology* **37**, 743–746.

Rieu R., Allen P., Etienne J., Cozzi A. and Wiechert U. (2006) A Neoproterozoic glacially influenced basin margin succession and "atypical" cap carbonate associated with bedrock palaeo-valleys, Mirbat area, southern Oman. *Basin Res.* **18**, 471–496.

Rothman D. H., Hayes J. M. and Summons R. E. (2003) Dynamics of the neoproterozoic carbon cycle. *PNAS* **100**, 8124–8129.

Sadler P. M. (1981) Sediment accumulation rates and the completeness of stratigraphic sections. *J. Geol.* **89**, 569–584.

Sahoo S. K., Planavsky N. J., Kendall B., Wang X., Shi X., Scott C., Anbar A. D., Lyons T. W. T. and Jiang G. G. (2012) Ocean oxygenation in the wake of the Marinoan glaciation. *Nature* **489**, 546–549.

Schröder S. and Grotzinger J. P. (2007) Evidence for anoxia at the Ediacaran–Cambrian boundary: the record of redox-sensitive trace elements and rare earth elements in Oman. *J. Geol. Soc. Lond.* **164**, 175–187.

Schrag D. P., Higgins J. A., Macdonald F. A. and Johnston D. T. (2013) Authigenic carbonate and the history of the global carbon cycle. *Science* **339**, 533–534.

Scott C., Lyons T. W., Bekker A., Shen Y., Poulton S. W., Chu X. and Anbar A. D. (2008) Tracing the stepwise oxygenation of the Proterozoic ocean. *Nature* **452**, 456–459.

Shen B., Xiao S., Kaufman A. J., Bao H., Zhou C. and Wang H. (2008a) Stratification and mixing of a post-glacial Neoproterozoic ocean: Evidence from carbon and sulfur isotopes in a cap dolostone from northwest China. *Earth Planet. Sci. Lett.* **265**, 209–228.

Shen Y. Y., Zhang T. T. and Hoffman P. F. P. (2008b) On the coevolution of Ediacaran oceans and animals. *Proc. Natl. Acad. Sci. U.S.A.* **105**, 7376–7381.

Shen B., Xiao S., Zhou C., Kaufman A. J. and Yuan X. (2010) Carbon and sulfur isotope chemostratigraphy of the Neoproterozoic Quanji Group of the Chaidam Basin, NW China: basin stratification in the aftermath of an Ediacaran glaciation postdating the Shuram event? *Precambr. Res.* **177**, 241–252.

Strauss H. (1997) The isotopic composition of sedimentary sulfur through time. *Palaeogeogr. Palaeoclimatol. Palaeoecol.* **132**, 97–118.

Strauss H. (1993) The sulfur isotopic record of Precambrian sulfates: new data and a critical evaluation of the existing record. *Precambr. Res.*, 225–246.

Veizer J., Holser W. T. and Wilgus C. K. (1980) Correlation of 13C/12C and 34S/32S secular variations. *Geochim. Cosmochim. Acta* **44**, 579–587.

Verdel C., Wernicke B. P. and Bowring S. A. (2011) The Shuram and subsequent Ediacaran carbon isotope excursions from southwest Laurentia, and implications for environmental stability during the metazoan radiation. *Geol. Soc. Am. Bull.* **123**, 1539–1559.

Wright V., Ries A. and Munn S. (1990) Intraplatformal basin-fill deposits from the Infracambrian Huqf Group, east Central Oman. In *The Geology and Tectonics of the Oman Region* (eds. A. Robertson, M. Searle and A. Ries). Geological Society, pp. 1–16.

Wu N., Farquhar J., Strauss H., Kim S.-T. and Canfield D. E. (2010) Evaluating the S-isotope fractionation associated with Phanerozoic pyrite burial. *Geochim. Cosmochim. Acta* **74**, 2053–2071.

Wu N., Farquhar J. and Fike D. A. (2015) Ediacaran Sulfur cycle: Insights from sulfur isotope measurements (Δ^{33}S and δ^{34}S) on paired sulfate-pyrite in the Huqf Supergroup of Oman. *Geochim. Cosmochim. Acta* **164**, 352–364.

Xiao S. (2004) Neoproterozoic glaciations and the fossil record. In *The Extreme Proterozoic: Geology, Geochemistry, and Climate* (eds. G. S. Jenkins, M. McMenamin, L. E. Sohl and C. P. McKay). American Geophysical Union, pp. 199–214.

Xiao S., McFadden K. A., Peek S., Kaufman A. J., Zhou C., Jiang G. and Hu J. (2012) Integrated chemostratigraphy of the Doushantuo Formation at the northern Xiaofenghe section (Yangtze Gorges, South China) and its implication for Ediacaran stratigraphic correlation and ocean redox models. *Precambr. Res.* **192–195**, 125–141.

Young G. M. (2013) Evolution of Earth's climatic system: evidence from ice ages, isotopes, and impacts. *GSAT*, 4–10.

Zhu M., Zhang J. and Yang A. (2007) Integrated Ediacaran (Sinian) chronostratigraphy of South China. *Palaeo* **254**, 7–61.

Associate editor: James Farquhar